Distributed and Multifaceted Effects of Threat and Safety

Dinavahi V. P. S. Murty[1], Songtao Song[1], Kelly Morrow[1], Jongwan Kim[2], Kesong Hu[3], and Luiz Pessoa[1]

Abstract

■ In the present fMRI study, we examined how anxious apprehension is processed in the human brain. A central goal of the study was to test the prediction that a subset of brain regions would exhibit sustained response profiles during threat periods, including the anterior insula, a region implicated in anxiety disorders. A second important goal was to evaluate the responses in the amygdala and the bed nucleus of the stria terminals, regions that have been suggested to be involved in more transient and sustained threat, respectively. A total of 109 participants performed an experiment in which they encountered "threat" or "safe" trials lasting approximately 16 sec. During the former, they experienced zero to three highly unpleasant electrical stimulations, whereas in the latter, they experienced zero to three benign electrical stimulations (not perceived as unpleasant). The timing of the stimulation during trials was randomized, and as some trials contained no stimulation, stimulation delivery was uncertain. We contrasted responses during threat and safe trials that did not contain electrical stimulation, but only the potential that unpleasant (threat) or benign (safe) stimulation could occur. We employed Bayesian multilevel analysis to contrast responses to threat and safe trials in 85 brain regions implicated in threat processing. Our results revealed that the effect of anxious apprehension is distributed across the brain and that the temporal evolution of the responses is quite varied, including more transient and more sustained profiles, as well as signal increases and decreases with threat. ■

INTRODUCTION

In humans, two types of threat-related processing in the brain have been investigated. Phasic processing is triggered by punctate cues, such as conditioned stimuli that are briefly presented. A large body of results reveals that multiple structures are engaged by conditioned stimuli, including the anterior insula, midcingulate cortex (MCC), thalamus, and, less consistently, the amygdala (Fullana et al., 2018). However, many forms of threat involve stressors that are uncertain, including temporal uncertainty. Anxious states induced by such unpredictable stressors have temporally extended and widespread effects on brain function (Hermans, Henckens, Joëls, & Fernández, 2014; McMenamin, Langeslag, Sirbu, Padmala, & Pessoa, 2014; Hermans et al., 2011; Thomason, Hamilton, & Gotlib, 2011; Kienast et al., 2008; Scott, Heitzeg, Koeppe, Stohler, & Zubieta, 2006). However, temporally extended threat remains poorly understood, including the question of whether or not responses are sustained during longer periods (Hur et al., 2020; McMenamin et al., 2014; Schlund, Hudgins, Magee, & Dymond, 2013; Somerville et al., 2013; Alvarez, Chen, Bodurka, Kaplan, & Grillon, 2011; Hasler et al., 2007). A central goal of this study was to test the prediction that a subset of brain regions would exhibit sustained response profiles during threat periods, including the anterior insula, a region implicated in anxiety disorders (Grupe & Nitschke, 2013; Paulus & Stein, 2006).

Whereas early work in rodents suggested that the amygdala plays a role in processing transient aversive stimuli (e.g., conditioned stimuli) and the bed nucleus of the stria terminalis (BST) is implicated in sustained "anxious/apprehensive" processing (Walker, Toufexis, & Davis, 2003; Davis & Shi, 1999), such proposed division of labor is now debated (Klumpers, Kroes, Baas, & Fernández, 2017; Paré & Quirk, 2017; Shackman & Fox, 2016; Tovote, Fadok, & Lüthi, 2015; Canteras, Resstel, Bertoglio, de Pádua Carobrez, & Guimaraes, 2009). Thus, a second important goal of this study was to test whether the response profile in these two regions is transient or sustained during threat anticipation states. Based on our previous studies, our working hypothesis was that only the BST would generate a sustained response profile (e.g., McMenamin et al., 2014).

It is well established that multiple brain regions generate stronger responses during threat compared with neutral conditions. However, growing evidence reveals that a complementary set of regions responds less strongly during threat relative to safe (for evidence in conditioning studies, see Fullana et al., 2018). For example, in a recent study, regions along the midline (including the posterior cingulate cortex [PCC]) showed decreased responses for proximal versus distal threat (Meyer, Padmala, & Pessoa, 2019), consistent with previous findings of the virtual

[1]University of Maryland College Park, MD, [2]Jeonbuk National University, South Korea, [3]Lake Superior State University, Sault Ste. Marie, MI

© 2022 Massachusetts Institute of Technology

Journal of Cognitive Neuroscience 34:3, pp. 495–516
https://doi.org/10.1162/jocn_a_01807

tarantula paradigm by Mobbs et al. (2010; see also (Yao, Qi, Kendrick, & Mobbs, 2018). It is noteworthy that many regions that exhibit greater responses during safe relative to threat overlap with the so-called default network. Thus, another important goal of the study was to test whether such regions always belong to the default network.

In this study, we studied 109 participants during a temporally uncertain threat paradigm (Figure 1). Our goal was to understand brain signals during periods of anxious anticipation. To do so, we contrasted responses during threat and safe trials that did not contain electrical stimulation, but only the potential that unpleasant (threat) or benign (safe) stimulation could occur. We estimated responses without making response-shape assumptions. Most studies of temporally extended threat assume that hemodynamic responses follow a canonical shape. Whereas this assumption is often reasonable for experimental paradigms with brief events, it is problematic when longer conditions are employed that generate responses that do not follow those based on the canonical shape (Sreenivasan & D'Esposito, 2019; Chen, Saad, Adleman, Leibenluft, & Cox, 2015). The ability to estimate response shape is particularly important when characterizing whether or not threat-related responses are transient (for discussion, see Hur et al., 2020).

Whole-brain fMRI analysis often lacks statistical power to uncover effects at the voxel level, which can lead to poor replicability (Cremers, Wager, & Yarkoni, 2017). Therefore, we performed most analyses at the ROI level by using Bayesian multilevel modeling (BML; McElreath, 2018; Gelman & Hill, 2006). One of the strengths of BML is that it allows the simultaneous estimation of multiple clustered parameters within a single model (in an educational setting, for example, the effects of different schools across a state). In the present context, BML allowed the estimation of the effects at each brain region while taking into consideration effects at other regions (note that the objective is distinct from that of performing network-related analysis). Although BML is not computationally feasible at the voxel level for the whole brain, we investigated voxelwise effects in the insula and amygdala given their importance in threat-related processing. For further information about our approach, see Chen et al. (2019) and Limbachia et al. (2021).

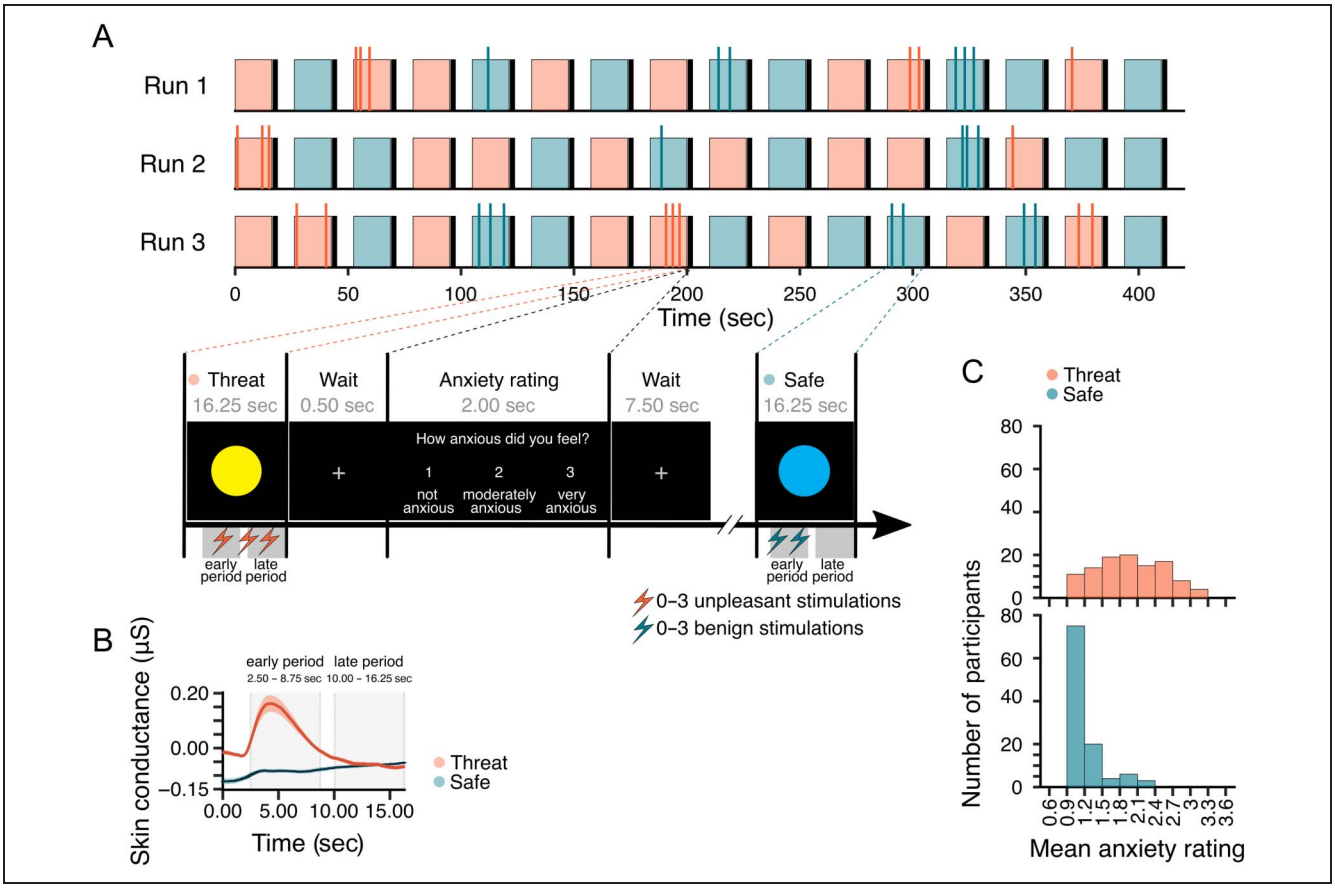

Figure 1. Paradigm description. (A) During threat trials (pink), participants could receive zero to three highly unpleasant electrical stimulations over a period of 16.25 sec, whereas during safe trials (blue), participants could receive zero to three benign electrical stimulations (not perceived as aversive). Actual stimulations are indicated by vertical line segments during trials. Our analyses focused on trials that did not contain electrical stimulation. At the end of each trial, participants rated their anxiety levels on a scale of 1–3, followed by a 7.50-sec fixation cross before the next block. (B) SCRs for threat and safe trials. Error bands show 95% interval for standard error across participants. (C) Anxiety rating during threat and safe trials.

METHODS

Participants

One hundred nine right-handed participants (53 women; ages 18–35 years, average = 21.17 years, *SD* = 2.59 years) with normal hearing, normal or corrected-to-normal vision, and no reported neurological disease or current use of psychoactive drug were recruited from the University of Maryland community. The study was approved by the University of Maryland institutional review board, and all participants provided written informed consent before participating in the study. All were paid immediately after the experiment ($10 per hour for assessments in the lab and $30 per hour for the MRI session).

Stimuli and Behavioral Paradigm

Before scanning, participants completed the Trait Anxiety portion of the Spielberger State–Trait Anxiety Inventory (Spielberger, Gorsuch, Lushene, Vagg, & Jacobs, 1970) and completed the State Anxiety portion immediately before scanning. To induce an anxious state, a threat of unpleasant shock paradigm was used while participants were scanned. The experiment consisted of three runs over a 2-hr session (Figure 1A). Each run consisted of eight threat and eight safe trials presented in random order. On each trial, a colored circle was presented for 16.25 sec via PsychoPy (www.psychopy.org). Before scanning, participants were informed that the color of the circle indicated whether a trial was "threat" (yellow circle) or "safe" (blue circle). A threat circle indicated that they could receive zero to three highly unpleasant, but not painful, electrical stimulations (referred to as "threat" here), whereas a safe circle indicated that they could receive zero to three very mild, but perceptible, electrical stimulations (referred to as "safe"); the latter were not reported as unpleasant by participants.

An electric stimulator (Coulbourn Instruments) delivered 500-msec stimulation to the fourth and fifth fingers of the left hand via MRI-compatible electrodes. Electrical stimulation levels were set by participants, as follows. To determine the "safe" level, an initial setting of 0.1 mA was increased by steps of 0.1 mA until the participant reliably felt minimal, "benign" stimulation. To determine the "threat" level, an initial setting of 1 mA was increased until the participant went as high as possible such that stimulation was "highly unpleasant" but not painful. Stimulation levels were set before the start of the experiment and repeated before the start of each run to prevent habituation. Across participants, the safe level ranged from 0.4 to 3.0 mA (mean = 0.94, *SD* = 0.42); a total of 16 participants recalibrated the safe level during the experiment. The threat level ranged from 1.4 to 10.0 mA (mean = 3.71, *SD* = 1.40); a total of 42 participants recalibrated the threat level during the experiment.

Of a total of 48 trials, 16 trials (8 threat and 8 safe) had at least one electrical stimulation; importantly, 32 trials (16 threat and 16 safe) contained no electrical stimulation. Thus, on a given trial, electrical stimulation was uncertain. The number of electrical stimulations per run was equated for safe and threat conditions. The sequence of trials and electrical stimulations were the same across participants (including the exact timing; Figure 1A illustrates the electrical stimulation events).

At the end of each trial, participants rated how anxious they felt on a scale of 1–3 (1 = *not anxious*, 2 = *moderately anxious*, and 3 = *very anxious*). Ratings were indicated by the participants via button press. Anxiety ratings were followed by a 7.5-sec fixation cross before the next trial. Rating data were unavailable for one participant. For the remaining participants, rating responses were not available for 2% of the trials because responses were not provided during the 2-sec window. The distribution of rating values is shown in Figure 1C. Note that, although we collected ratings, we did not use them in the analysis of fMRI data because they were highly correlated with trial condition, so they did not carry independent information (participants mostly rated safe trials a level of 1 and threat trials a level greater than 1; see Figure 1C).

MRI Data Acquisition

MRI data collection used a 3-T Siemens TRIO scanner (Siemens Medical Systems) with a 32-channel head coil. First, we acquired a high-resolution T1-weighted MPRAGE anatomical scan (repetition time [TR] = 2400 msec, echo time [TE] = 2.01 msec, field of view = 256 mm, voxel size = 0.8 mm isotropic). Subsequently, we collected functional EPI volumes over three runs (340 images per run) using a multiband scanning sequence with TR = 1250 msec, TE = 39.4 ms, field of view = 210 mm, and multiband factor = 6. Each volume contained 66 nonoverlapping oblique slices oriented 30° clockwise relative to the AC–PC axis; thus, voxels were 2.2-mm isotropic. Double-echo field maps (TE = 73.0 msec) were also acquired with acquisition parameters matched to the functional data.

Skin Conductance Response Acquisition

Skin conductance responses (SCRs) were collected using the MP-150 data acquisition system (BIOPAC Systems, Inc.) with the GSR100C module. Signals were acquired at 250 Hz using MRI-compatible electrodes attached to the index and middle fingers of the participants' nondominant, left hand. SCR data from two participants (one woman and one man) were not collected because of technical problems.

ROIs

We focused on 85 structurally and functionally defined cortical and subcortical ROIs (Figure 2). Tables 1 and 2 provide complete information of ROI sources. Functional masks were based on data from separate studies, not the

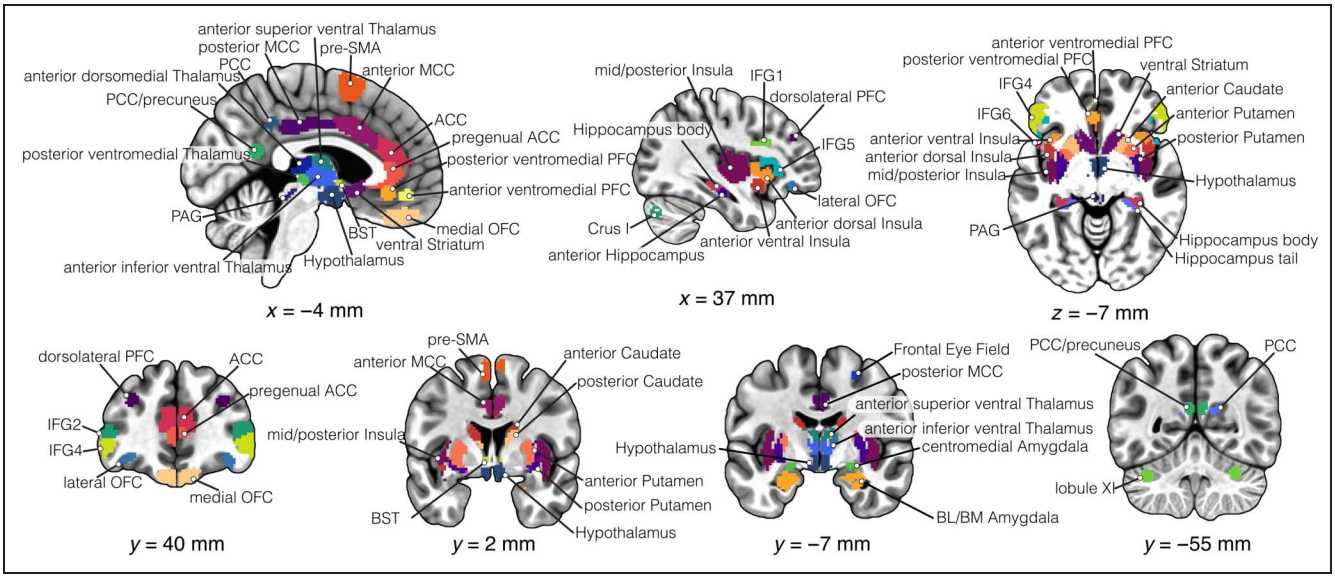

Figure 2. Regions of interest. ACC = anterior cingulate cortex; BL/BM = amygdala; BST = bed nucleus of the stria terminalis; IFG = inferior frontal gyrus; MCC = mid- cingulate cortex; OFC = orbitofrontal cortex, PAG = periaqueductal gray; PCC = posterior cingulate cortex; PFC = prefrontal cortex; pre-SMA = pre-supplementary motor area.

present one. Potential contributions of white matter and cerebrospinal fluid were minimized by excluding voxels that intersected with masks of these tissue types. All ROIs were disjoint, such that no overlap occurred between them.

Data Preprocessing

Functional images were preprocessed as described in our previous work by using a combination of fMRI packages and in-house scripts (Limbachia et al., 2021). Slice-timing correction was performed with the Analysis of Functional Neuroimages (AFNI; Cox, 1996) *3dTshift* with Fourier interpolation to align the onset times of each slice in a volume to the first acquired slice. For voxelwise analysis (but not ROI level), data were spatially smoothed with a Gaussian filter (4 mm FWHM) restricted to gray matter voxels. Signal intensity at each voxel was normalized to a mean value of 100 separately for each run. To further reduce the contribution of head motion artifacts, FSL's Independent Component Analysis, Automatic Removal of Motion Artifacts toolbox was applied (Pruim, Mennes, Buitelaar, & Beckmann, 2015). Components classified as head motion were regressed out of the data using FSL's *fsl_regfilt*.

Given the small size of some of our ROIs, following previous work (Limbachia et al., 2021), we sought to improve coregistration between functional and anatomical images using a "voting scheme" to determine whether or not a voxel belonged to the brain (i.e., skull stripping). To do so, we employed six different fMRI packages (ANTs: Avants, Tustison, & Song, 2009; AFNI: Cox, 1996; SPM: Friston, Ashburner, Kiebel, Nichols, & Penny, 2007; ROBEX: Iglesias, Liu, Thompson, & Tu, 2011; BrainSuite: Shattuck & Leahy, 2002; FSL: Smith et al., 2004). Based on T1 structural data, if four of six packages estimated a voxel to belong to the brain, it was retained, otherwise it was discarded. Next, ANTs was used to estimate a nonlinear transformation mapping the skull-stripped anatomical T1 image to the skull-stripped MNI152 template(interpolated to 1-mm isotropic voxels). The nonlinear transformations from coregistration/unwarping and normalization were combined into a single transformation that was applied to map volume-registered functional volumes to standard space (interpolated to 2-mm isotropic voxels).

Preprocessed functional data were then subjected to runwise head motion evaluation. Any particular run was excluded if motion estimates exceeded a mean framewise displacement of 0.5 mm, had a total framewise displacement of 5 mm or more, or had 20% or more of all TRs with framewise displacement over 0.5 mm. Runs were then concatenated for each subject.

We evaluated potential differences in residual head motion after head motion correction (in other words, were any differences still present after motion correction?). We did so because potential differences in residual motion could in principle be a factor driving differential responses. We focused on the temporal analysis window used for the fMRI analysis and computed the framewise displacement over safe and threat periods (see below); as in the fMRI analysis, we considered trials with no electrical stimulation. Framewise displacement sums the absolute value of movements in the three linear (superior–inferior, right–left, and anterior–posterior) and angular (roll, pitch, and yaw) dimensions (Power et al., 2014). Average residual framewise displacement difference between threat and safe trials was only 5.1% of a voxel dimension (2.2 mm) per run (threat < safe). Although this difference was statistically significant ($p < .001$, permutation test),

Table 1. Cortical ROIs

Region	*Type*	*Voxel Extent (R, L)*	*Origin*	*Description*
Medial OFC	Probalistic	407, 339	Julich Brain atlas; Amunts et al. (2020); Wojtasik et al. (2020)	Probability threshold = .60, midline clipped
Lateral OFC	Probalistic	56, 62	Julich Brain atlas; Amunts et al. (2020); Wojtasik et al. (2020)	Probability threshold = .60
Anterior ventromedial PFC	Functional	67	Meyer et al. (2019)	5-mm sphere of threat proximity cluster
Posterior ventromedial PFC	Functional	81	Boeke et al. (2017)	5-mm sphere based on coordinates
IFG 1	Probalistic	329, 304	Brainnetome atlas; Fan et al. (2016)	
IFG 2	Probalistic	293, 337	Brainnetome atlas; Fan et al. (2016)	
IFG 3	Probalistic	313, 264	Brainnetome atlas; Fan et al. (2016)	
IFG 4	Probalistic	349, 323	Brainnetome atlas; Fan et al. (2016)	
IFG 5	Probalistic	525, 434	Brainnetome atlas; Fan et al. (2016)	
IFG 6	Probalistic	260, 261	Brainnetome atlas; Fan et al. (2016)	
Dorsolateral PFC	Functional	75, 75	Hur et al. (2020)	5-mm sphere based on threat > safe coordinates
Frontal eye field	Functional	81, 33	Toro et al. (2008)	5-mm spheres based on report MNI coordinates
Anterior ventral insula	Probalistic	176, 171	Hammers atlas; Faillenot et al. (2017)	Probability threshold = .50; anterior pole mask
Anterior dorsal insula	Probalistic	235, 236	Hammers atlas; Faillenot et al. (2017)	Probability threshold = .50; anterior short and middle short gyri union
Mid/posterior Insula	Probalistic	572, 533	Hammers atlas; Faillenot et al. (2017)	Probability threshold = .50; posterior short, anterior long, and posterior long gyri union
Pregenual anterior cingulate	Structural	143, 137	Desikan-Killany atlas; Desikan et al. (2006)	Overlap with vmPFC and ACC excluded; midline excluded
ACC	Structural	346, 364	Brainnetome atlas; Fan et al. (2016)	overlap with aMCC excluded; midline excluded
Anterior MCC	Structural	382, 302	Destrieuxet al. (2010)	Midline excluded
Posterior MCC	Structural	369, 245	Desikan-Killany atlas; Desikan et al. (2006)	Overlap with aMCC excluded; midline excluded
Medial PCC	Functional	64	Meyer et al. (2019)	Based on previous functional data
PCC	Functional	52, 34	Meyer et al. (2019)	Based on previous functional data
PCC/precuneus	Functional	60, 57	Meyer et al. (2019)	Based on previous functional data
Pre-SMA	Probalistic	227, 213	Julich Brain atlas; Amunts et al. (2020); Ruan et al. (2018)	Probability threshold = .50; midline excluded

Notes to All ROI masks were multiplied with a gray matter mask to reduce contribution of cerebrospinal fluid and white matter in data. L = left; R = right.

Table 2. Subcortical ROIs

Region	*Type*	*Voxel Extent (R, L)*	*Origin*	*Description*
Ventral striatum	Functional	241, 300	Pauli et al. (2016)	
Anterior caudate	Functional	488, 364	Pauli et al. (2016)	
Posterior caudate	Functional	124, 214	Pauli et al. (2016)	
Anterior putamen	Functional	339, 346	Pauli et al. (2016)	
Posterior putamen	Functional	268, 239	Pauli et al. (2016)	
BST	Structural	8, 9	Theiss et al. (2017)	
Centromedial amygdala	Structural	45, 35	Nacewicz et al. (2014)	Combination of central and medial amygdala masks
BL/BM amygdala	Structural	129, 132	Nacewicz et al. (2014)	Combination of basolateral and basomedial amygdala masks
Anterior hippocampus	Functional	333, 331	Melbourne subcortical atlas; Tian et al. (2020)	Scale 3 of Melbourne atlas (second finest parcellation)
Hippocampus body	Functional	192, 190	Melbourne subcortical atlas; Tian et al. (2020)	Scale 3 of Melbourne atlas
Hippocampus tail	Functional	92, 102	Melbourne subcortical atlas; Tian et al. (2020)	Scale 3 of Melbourne atlas
Hypothalamus	Structural	169, 170	Pauli et al. (2018)	
Anterior superior ventral thalamus	Functional	161, 122	Melbourne subcortical atlas; Tian et al. (2020)	Scale 3 of Melbourne atlas
Anterior inferior ventral thalamus	Functional	244, 190	Melbourne subcortical atlas; Tian et al. (2020)	Scale 3 of Melbourne atlas
Posterior ventrolateral thalamus	Functional	16, 20	Melbourne subcortical atlas; Tian et al. (2020)	Scale 3 of Melbourne atlas
Posterior ventromedial thalamus	Functional	79, 82	Melbourne subcortical atlas; Tian et al. (2020)	Scale 3 of Melbourne atlas
Anterior dorsolateral thalamus	Functional	49, 77	Melbourne subcortical atlas; Tian et al. (2020)	Scale 3 of Melbourne atlas
Anterior dorsomedial thalamus	Functional	171, 170	Melbourne subcortical atlas; Tian et al. (2020)	Scale 3 of Melbourne atlas
PAG	Structural	15, 24	Ezra et al. (2015)	
Lobule XI (cerebellum)	Functional	109, 122	Hur et al. (2020);see map: https://identifiers.org/neurovault.collection:8583	6-mm spheres created from uncertain threat > uncertain safe functional map
Crus I (cerebellum)	Functional	105, 119	Krienen & Buckner (2009)	6-mm spheres created from peak coordinates

All ROI masks were multiplied with a gray matter mask to reduce contribution of cerebrospinal fluid and white matter in data. L = left; R = right.

the difference was very small in absolute terms. Furthermore, the original head motion parameters were used as covariates of no interest in our multiple regression models (see below). Together, although threat trials exhibited less head motion compared with safe, we do not believe this difference was a factor driving the results reported in the article.

Temporal signal-to-noise ratio, defined as the ratio of mean to standard deviation across time, can be rather low in some brain areas, including the OFC, amygdala, and periaqueductal gray (PAG). Voxels were excluded if their mean (after signal normalization to 100) was outside the range 95–105 or the standard deviation exceeded 25. Voxels that did not meet our criteria were discarded from the analysis (mean = 0.21, *SD* = 0.47% of voxels).

Subject-level Analysis

To estimate the shape of the responses during threat and safe trials, we focused on the 16 trials of each trial type with no electrical stimulation. Response shape was estimated by employing a series of cubic spline basis functions (similar to the "finite impulse response" method). The analysis utilized subject-level multiple linear regression with AFNI's *3dREMLfit* program.

At the ROI level, the analysis employed the average time series (unsmoothed data) across ROI voxels. At the voxel level, spatially smoothed data were used to increase signal to noise, as routinely done in fMRI analysis. Trials of a given type were modeled with 14 regressors (i.e., cubic splines) aligned to the trial onset (starting at $t = 0$ and ending at $t = 16.25$).

The anxiety rating period, which was not of interest here, was modeled by convolving a square wave with a canonical hemodynamic response. Likewise, the remaining trials containing at least one stimulation event were modeled by convolving the trial duration (16.25 sec) with a canonical filter. To minimize contamination of task-related signal with electrical stimulation events, the 15-sec period following each stimulation was censored from analysis. All analyses included a set of regressors modeling head motion parameters (six rigid body motion parameters and their discrete temporal derivatives), in addition to linear and nonlinear polynomial terms (up to third order) to account for baseline and slow signal drift.

A separate analysis was performed to estimate the responses to electrical stimulation events to confirm the presence of robust responses in regions like the amygdala (Figure 3). In this case, the cubic spline regressors were aligned to the electrical stimulation onset. Note that this was the only analysis containing trials with actual electrical stimulation (safe and threat).

Group Bayesian Multilevel Analysis: ROI Level

Employing a "single multilevel" model allowed the contributions of subject-level effects (i.e., subject effect across conditions) and ROI-level effects (i.e., ROI effect across subjects) to be estimated simultaneously with the condition effect (threat vs. safe). The input to the model consisted of 85 averaged-across-voxels time series from the first level described above, as in our previous work (Limbachia et al., 2021). The model was estimated using the *brms* R package (Bürkner, 2017), which utilizes *rstan* (https://mcstan.org/users/interfaces/rstan), the R interface to the Stan probabilistic language (https://mc-stan.org).

We considered two temporal time windows: early (2.5–8.75 sec from trial onset) and late (10–16.25 sec);

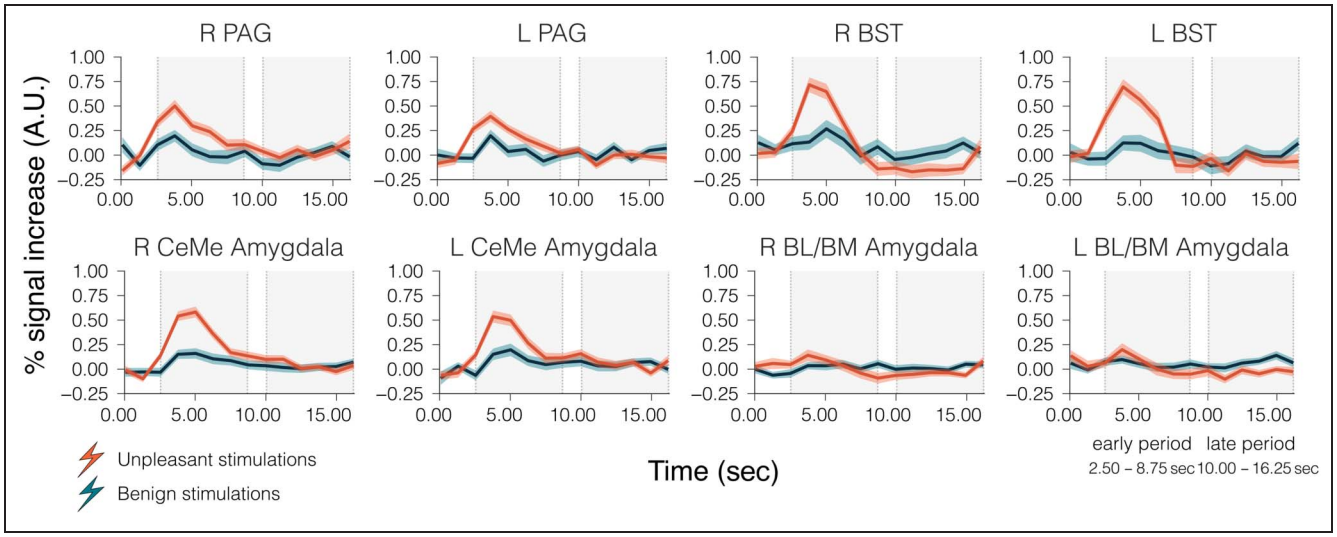

Figure 3. Hemodynamic responses to trials containing electrical stimulation. Estimated responses averaged across participants. Error bands show 95% interval for standard error across participants to illustrate variability only. Shaded regions represent early and late periods. L = left; R = right; CM = centromedial; BL/BM = basolateral/basomedial.

responses at 0 and 1.25 sec were not used to account for the latency of the hemodynamic response. For each window, we defined response magnitude as the sum of the responses across the window. In doing so, our goal was to create something akin to an "area under the curve" response measure (Chen et al., 2015). Given our within-subject design, we used the difference between threat and safe response magnitudes as the variable to be tested: $D_{s,r}$, where s indexes subjects and r indexes ROI. For computational expediency, we analyzed the two time windows "separately," taking into account anxiety-related covariates. In standard linear mixed-effects modeling notation, our model (Model 1) was defined as

$$D_{s,r} \sim 1 + \text{State} + \text{Trait} + (1|\text{Sub}) + (1 + \text{State} + \text{Trait}|\text{ROI})$$

where Sub (subject) and ROI are grouping variables. State and Trait indicate the covariates of the model. The terms "1" indicate intercept terms, including an overall intercept and so-called varying intercepts per subject (subject-specific contribution) and per ROI (ROI-specific contribution). The notation (1 + State + Trait|ROI) summarizes the varying intercepts and slopes per ROI, but also the correlation structure between intercept and slopes.

In a separate model (Model 2), we also modeled trial "period" to allow the explicit comparison between early and late periods:

$$D_{s,r,p} \sim 1 + \text{Period} + \text{State} + \text{Trait} + (1 + \text{Period}|\text{Sub}) + (1 + \text{Period} + \text{State} + \text{Trait}|\text{ROI})$$

where the definitions are the same as above, and p is a categorical variable indicating "early" or "late." Note that whereas it was possible to define a single model merging Models 1 and 2 above, it would have been extremely computationally demanding. Accordingly, we opted for the approach with two models described here.

Model estimation generates a single posterior that is a joint distribution in a high-dimensional parameter space. Posteriors for each effect at the ROI level were calculated by summing the relevant contributions (i.e., overall intercept term and intercept at the ROI level). Note that whereas posteriors can be plotted separately for each ROI for visualization purposes (Figure 4), they should be understood as belonging to a single joint distribution.

Bayesian estimation requires the specification of prior distributions for all the parameters of interest in the model. We employed so-called weakly informative priors that help estimation convergence (all $\hat{R} < 1.1$, as recommended) but have negligible impact on estimated parameters, especially with reasonable sample sizes. We provide a complete description of the Bayesian formulation of the model, together with the priors, in the following GitHub page: https://github.com/LCE-UMD/mood-anxiety.

Group Bayesian Multilevel Analysis: Voxel Level

We performed voxelwise BML analysis of insula and amygdala data separately. The analysis entailed adding a voxel level to the model above. In addition, instead of using the original ROI definitions, we created finer parcellations for the insula and amygdala. Thus, the 941 voxels of the entire left insula were clustered into 11 ROIs, and the 986 voxels of entire right insula were clustered into 10 ROIs. Similarly, the 167 voxels of the entire left amygdala were clustered into six ROIs, and the 176 voxels of entire right amygdala were clustered into six ROIs. In all cases, the new smaller ROIs respected the original ROI boundaries investigated in the region-level analysis (e.g., new insula ROIs did not include voxels from both the ventral and dorsal insula or correspondingly from the centromedial and the basolateral amygdala). Smaller ROIs were created by clustering adjacent voxels based on their $\{x, y, z\}$ coordinates (not time series data) with standard k-means clustering. The motivation for having finer parcellations of the insula and amygdala was related to the concept of partial pooling in multilevel modeling. By having a larger number of ROIs, the pooling effect (i.e., voxel effects possibly being pushed to some extent to the overall average of the ROI) was more strongly restricted to the local ROI to which a voxel belonged, thus respecting the idea that information exchange should tend to stay local.

The modeling approach to test the effect of trial type (Model 1) followed the same strategy as that of the ROI-level analysis, with the addition of the voxel-level data. The relatively small number of voxels in the amygdala allowed us to include a factor for "hemisphere" too:

$$D_{s,h,r,v} \sim 1 + \text{State} + \text{Trait} + (1|\text{Sub}) + (1|\text{Hem}) + (1|\text{ROI}) + (1|\text{VOX})$$

where s, h, r, and v indexed subject, hemisphere, sub-ROI, and voxel, respectively. To evaluate the effect of trial period, the corresponding Model 2 was:

$$D_{s,h,r,v,p} \sim 1 + \text{Period} + \text{State} + \text{Trait} + (1 + \text{Period}|\text{Sub}) + (1 + \text{Period}|\text{Hem}) + (1 + \text{Period}|\text{ROI}) + (1 + \text{Period}|\text{VOX})$$

where p indicated "early" or "late."

The number of voxels in the insula was sufficiently large that we were unable to apply the same approach used for the amygdala. For the insula, we were able to include covariates related to state/trait individual differences, and evaluate the effect of trial type at the voxel level:

$$D_{s,r,v} \sim 1 + \text{State} + \text{Trait} + (1|\text{Sub}) + (1|\text{ROI}) + (1|\text{VOX})$$

Convergence of estimates was observed in all cases ($\hat{R} < 1.1$, as recommended).

Skin Conductance

We adopted the same preprocessing approach used in our previous studies (e.g., Limbachia et al., 2021). For each

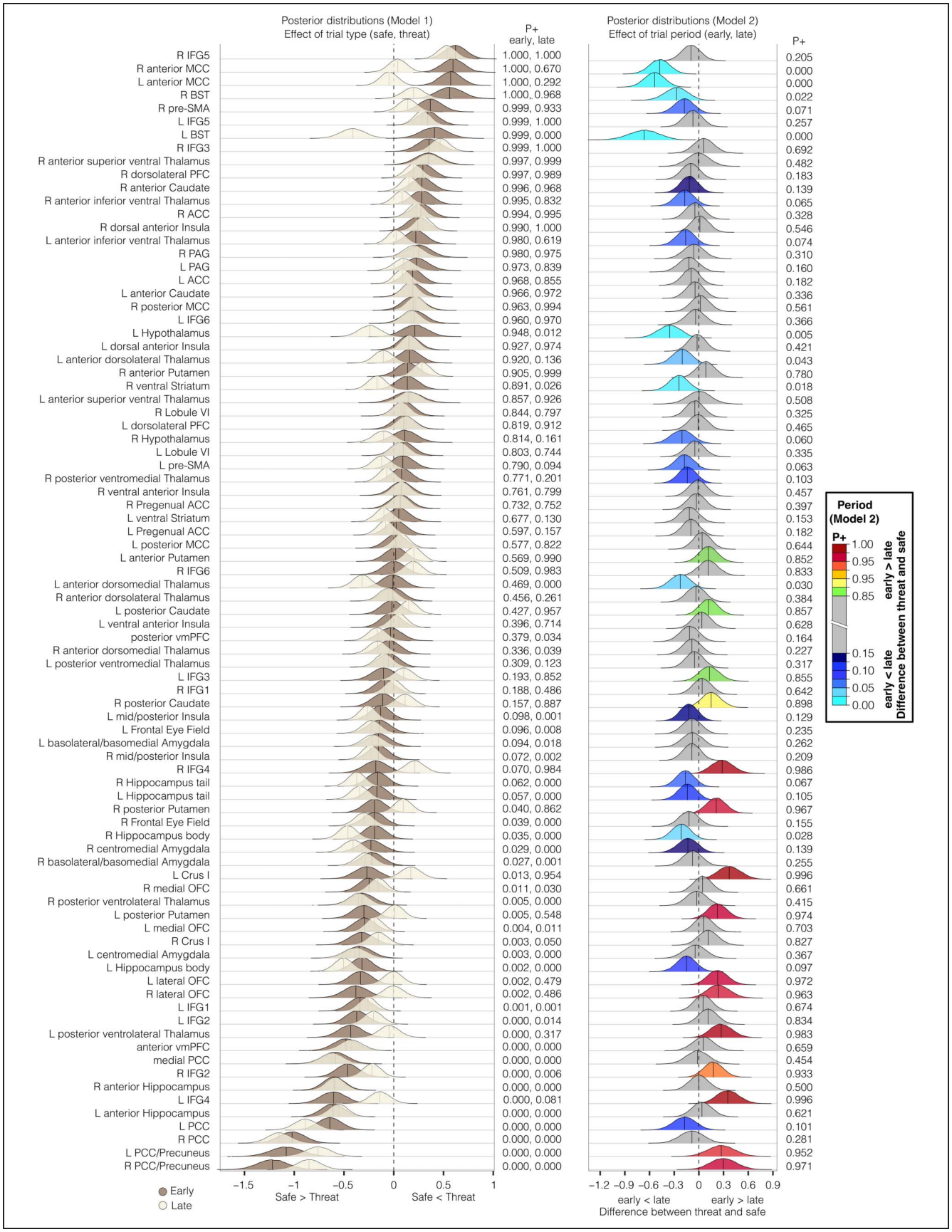

Figure 4. Posterior distributions. Left: Posteriors show the distribution of the trial type effect, namely, difference between threat and safe for the early (dark) and late (light) periods. Right: Posteriors show the distribution of the trial period effect, namely, difference between early and late for the trial type effect (difference between threat and safe). $p+$ is the probability that the effect is greater than zero.

run, we detrended the signal by removing the best linear fit to the data. Subsequently, we applied a median filter over 50-sample windows (200 msec) to remove high-frequency noise. Average responses during safe and threat trials were compared for the early and late periods separately. Statistical tests were performed via permutation testing (99,999 iterations), taking into consideration within-participant differences.

RESULTS

In this study, participants performed a threat-of-shock experiment (Figure 1A) during fMRI scanning. Participants experienced safe and threat trials during which they could receive temporally uncertain benign or unpleasant electrical stimulation, respectively, including "no stimulation." Given our interest in evaluating transient/sustained responses, we considered "early" and "late" temporal windows during the trial (participants were not aware of the analysis windows) and determined the effect of trial type in these windows separately. An effect of trial type (threat vs. safe) during early and/or late windows was used to inform whether threat-related responses were better conceptualized as transient or sustained. Unless explicitly stated, all safe and threat trials analyzed contained no electrical stimulation; in other words, they were trials during which the participant was aware that there was the possibility of a stimulation but did not contain stimulation.

SCRs and Anxiety Ratings

We observed a sizeable increase in skin conductance following the onset of threat trials but not safe trials (Figure 1B). Statistically, a clear effect of trial type was present during the early period ($p < .001$, permutation test), whereas it was not detected during the late period ($p = .448$, permutation test). Mean anxiety ratings were higher for threat trials (2.08 ± 0.05) compared with safe trials (1.25 ± 0.03; Figure 1C; $p < .001$, permutation test).

ROI-level Analysis

First, we confirmed that unpleasant physical stimulation evoked clear hemodynamic responses in a select group of regions. Indeed, we observed large, transient responses in the centromedial amygdala, PAG and BST (Figure 3). Next, we analyzed the responses to safe and threat trials in the complete set of ROIs (Figure 2). Recall that such trials did not have electrical stimulation and only differed in terms of the cue signaling trial type. For each ROI, we

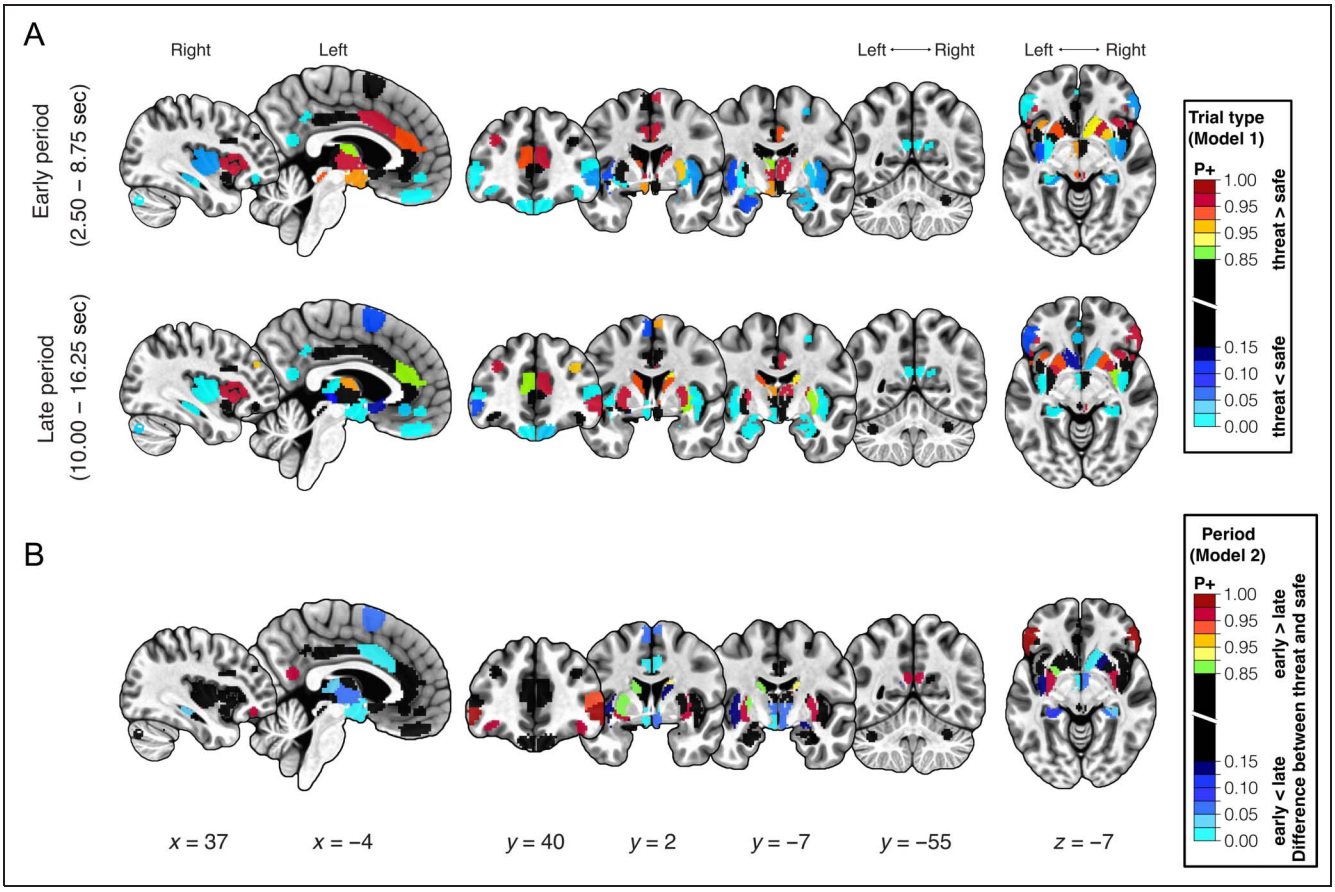

Figure 5. Effects of trial type and trial period. (A) Effect of trial type. Warmer colors indicate threat > safe, and cooler colors indicate the reverse. (B) Effect of trial period. Warmer colors indicate early > late trial type effect, and cooler colors indicate the reverse. Brain slices correspond to those in Figure 2.

considered the average response from each time window (early or late separately) as the response strength for a given condition and performed Bayesian multilevel analysis to test for a condition effect. We summarized statistical evidence in terms of $p+$ values (the probability that the effect is greater than zero) based on the posterior distribution; $p+$ values closer to 1 provide evidence that the difference is greater than 0 (threat > safe), whereas values

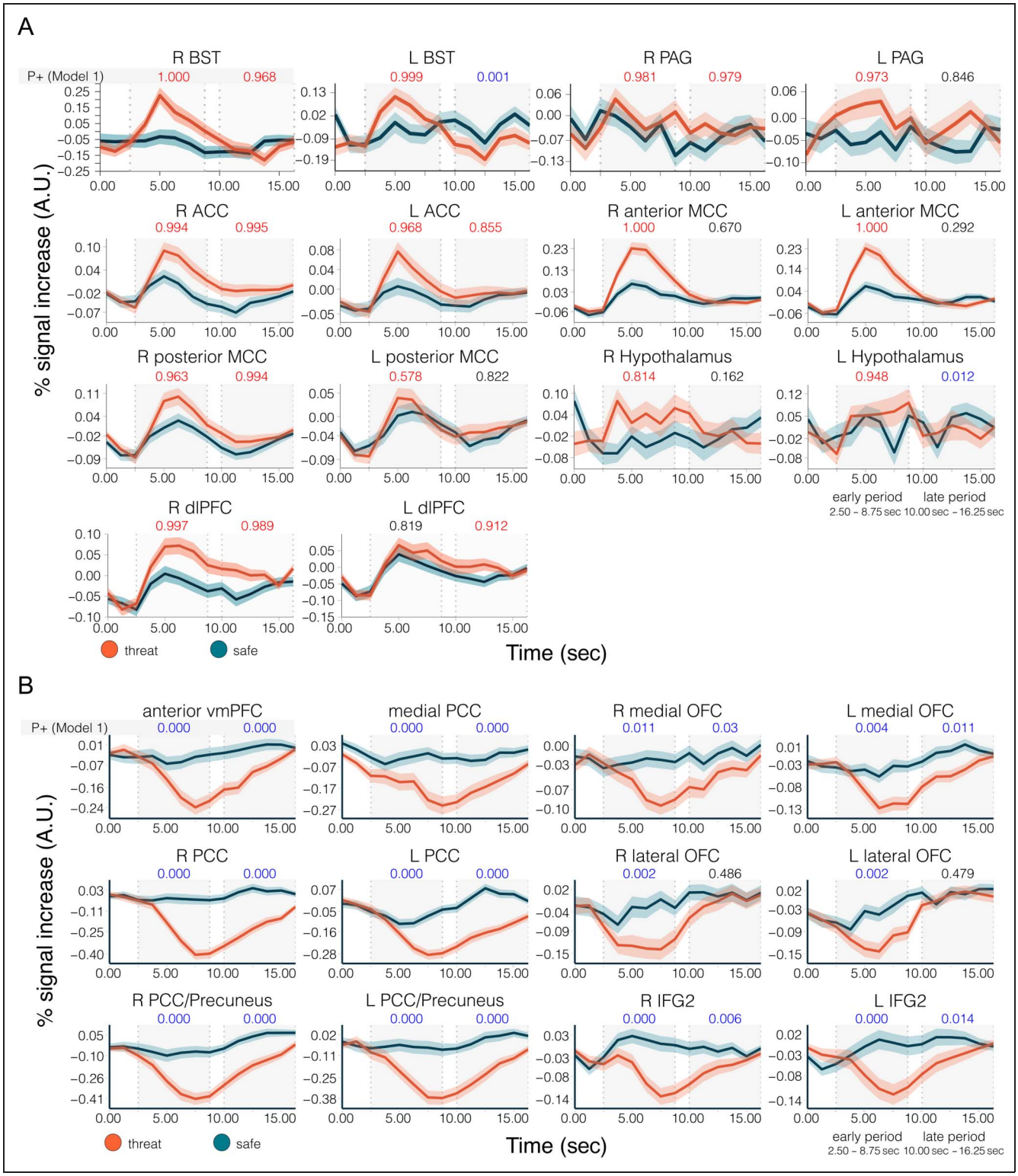

Figure 6. Estimated responses across key regions. Error bands show 95% interval for standard error across participants to illustrate variability only. Shaded regions indicate early and late periods. Numerical values indicate $p+$ (colored font highlights the strongest effects).

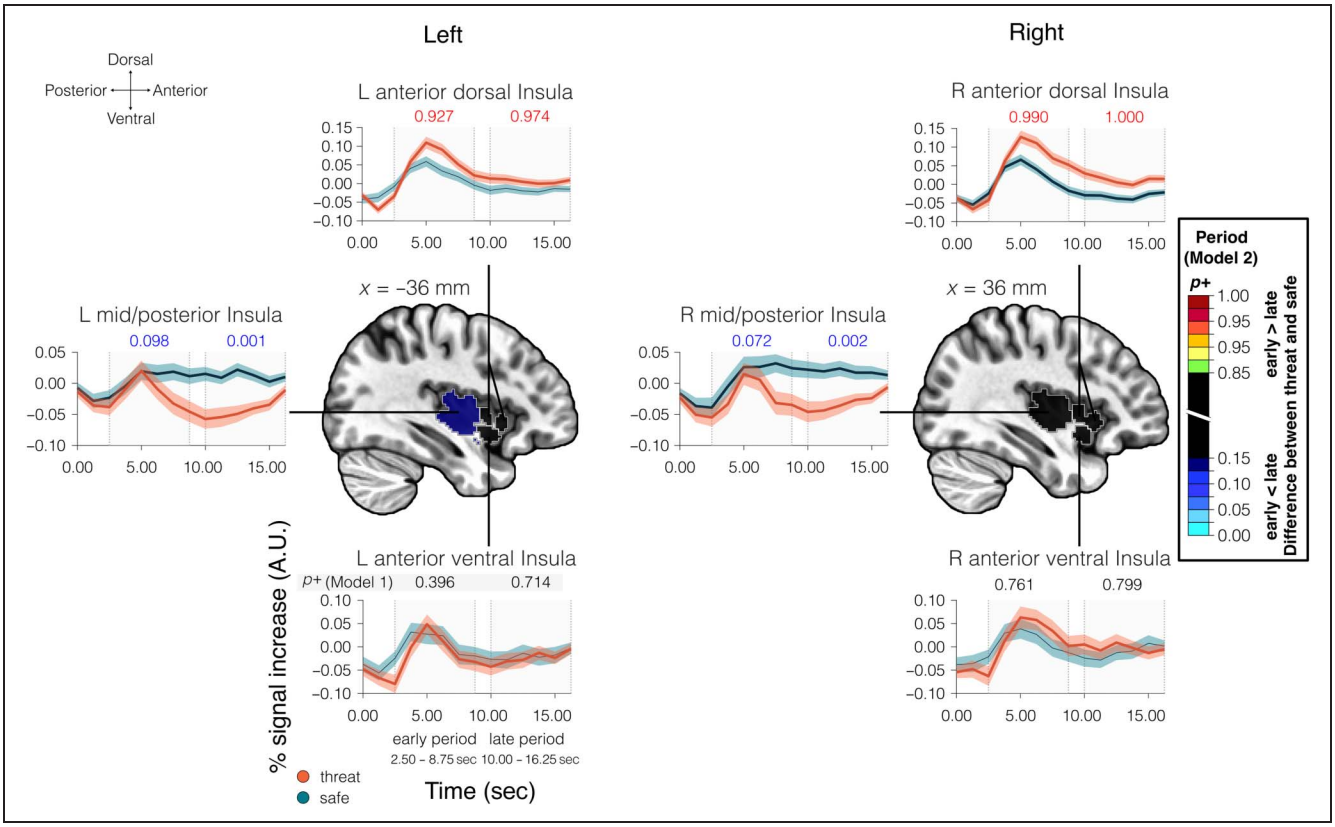

Figure 7. Estimated responses in the insula (ROI level). Error bands show 95% interval for standard error across participants to illustrate variability only. Shaded regions indicate early and late periods. The strength of the effect of trial type is indicated separately for the early and late periods (see $p+$ values; colored font highlights the strongest effects). The effect of trial period is indicated via color coding of the ROIs (see color scale).

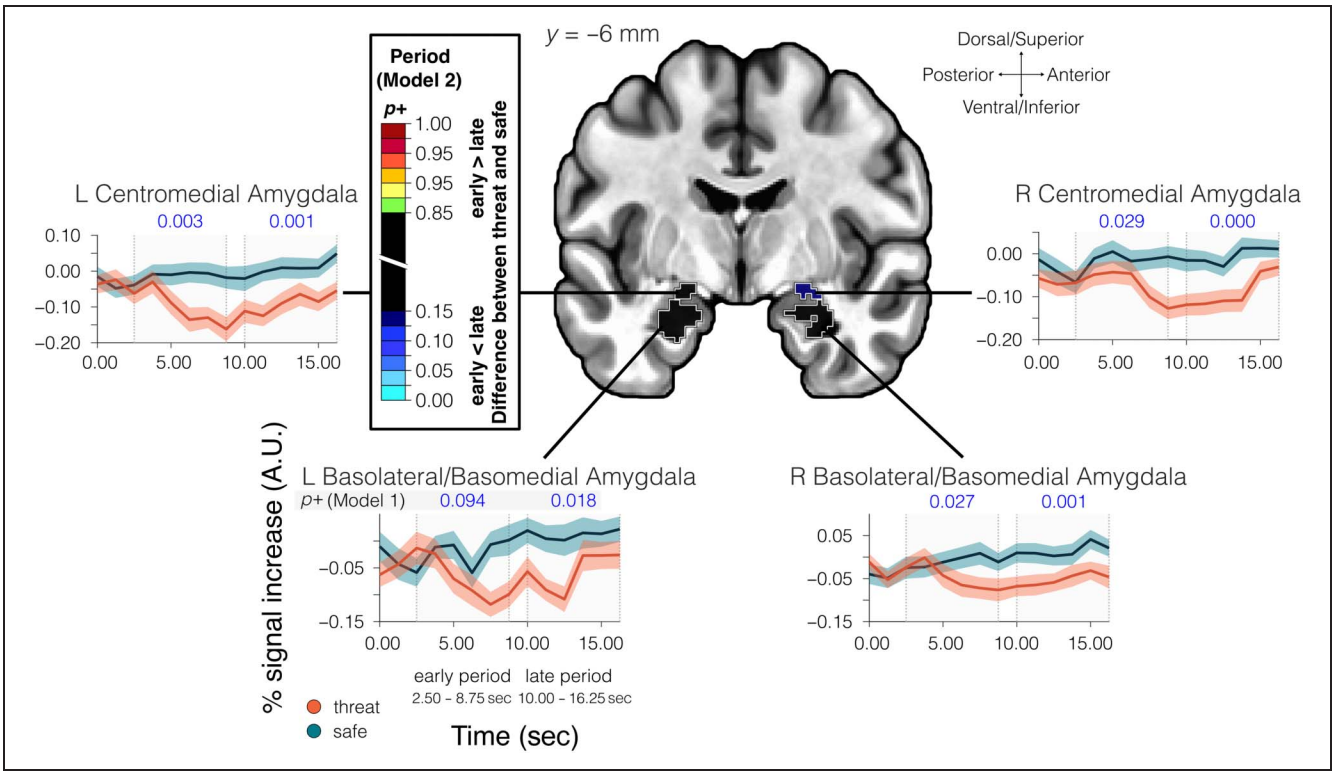

Figure 8. Estimated responses in the amygdala (ROI level). Error bands show 95% interval for standard error across participants to illustrate variability only. Shaded regions indicate early and late periods. The strength of the effect of trial type is indicated separately for the early and late periods (see $p+$ values; colored font highlights the strongest effects). The effect of trial period is indicated via color coding of the ROIs (see color scale).

closer to zero convey support for the inverse effect (threat < safe). We treat Bayesian probability values as providing a continuous amount of support for a given hypothesis, thus not dichotomously as "significant" versus "not significant." For presentation purposes, here we set thresholds of $p+ \geq .85$ (threat > safe) and $p+ \leq .15$ (threat < safe). Because BML implements "partial pooling" of information across regions as well as participants (and voxels for voxelwise analyses), the process tends to generate estimates that are more "conservative." For example, they will be closer to the average effect than if each region's effect were estimated individually. Effectively, the approach allows information to be shared across spatial units and tends to stabilize estimates. Because of this conservative nature, some statisticians have suggested that adjustment for multiple comparisons is not needed (Gelman, 2009), especially because all the inferences are drawn from a single, overall posterior distribution of an integrative model (for a detailed discussion, see Chen et al., 2021).

Figures 4 and 5 show the complete results in terms of posterior distributions and on brain slices, respectively. We observed very strong support (e.g., $p+ > .990$) for a threat > safe effect in early and/or late periods for multiple regions; very strong support in the opposite direction ($p+$ values very close to 0) was also observed. An explicit comparison between differential responses during early

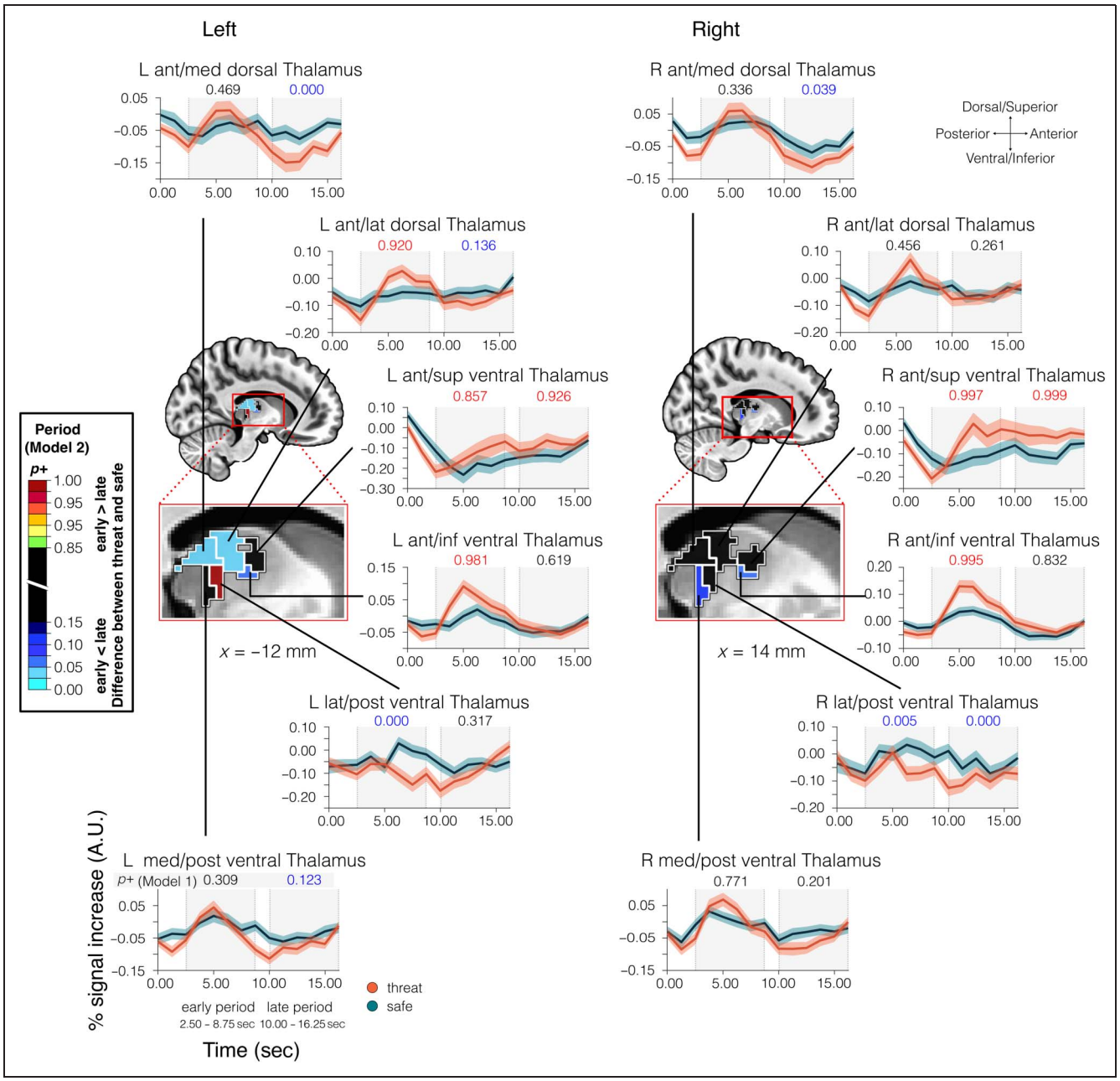

Figure 9. Estimated responses in the thalamus (ROI level). Error bands show 95% interval for standard error across participants to illustrate variability only. Shaded regions indicate early and late periods. The strength of the effect of trial type is indicated separately for the early and late periods (see $p+$ values; colored font highlights the strongest effects). The effect of trial period is indicated via color coding of the ROIs (see color scale).

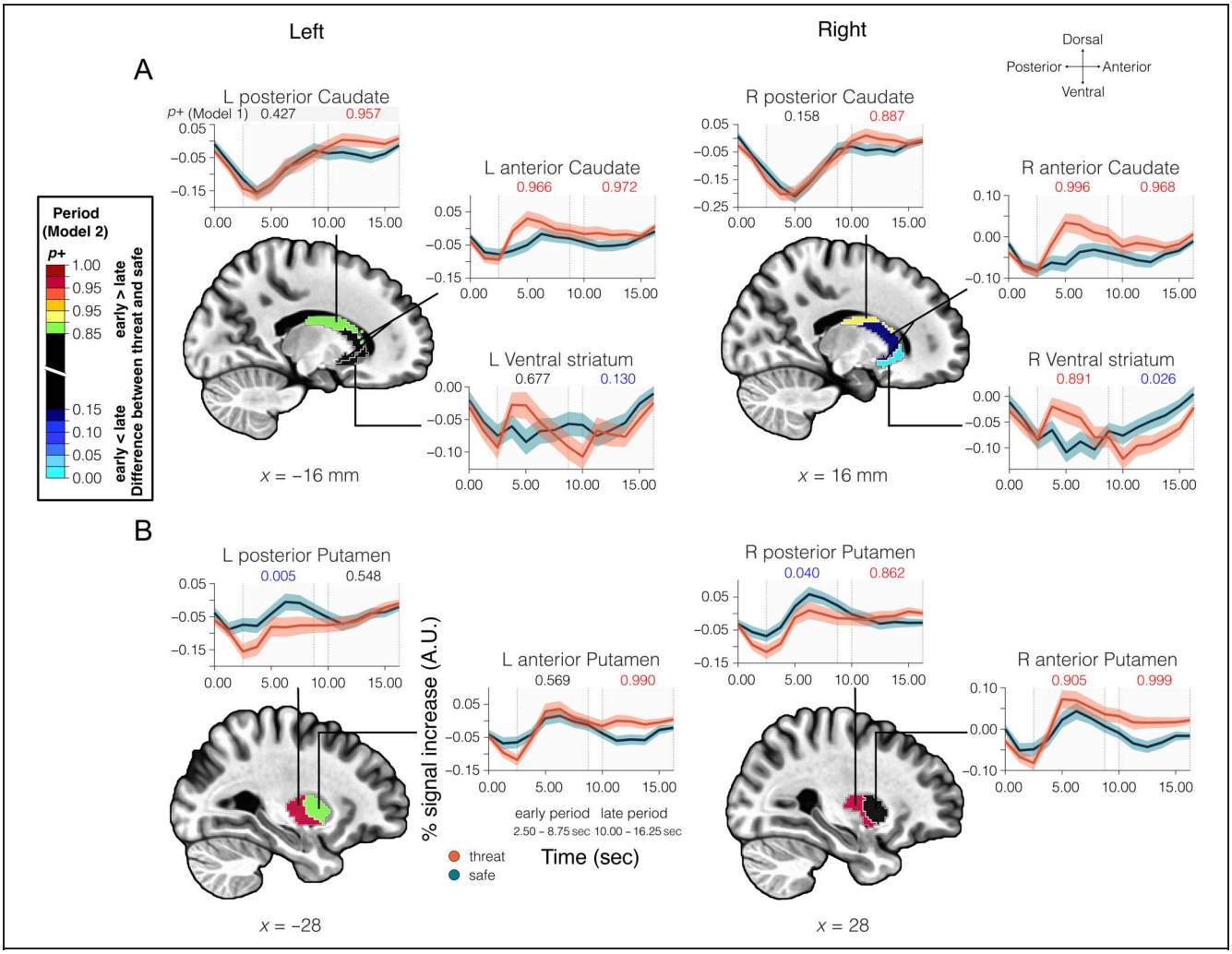

Figure 10. Estimated responses in the striatum (ROI level). Error bands show 95% interval for standard error across participants to illustrate variability only. Shaded regions indicate early and late periods. The strength of the effect of trial type is indicated separately for the early and late periods (see $p+$ values; colored font highlights the strongest effects). The effect of trial period is indicated via color coding of the ROIs (see color scale).

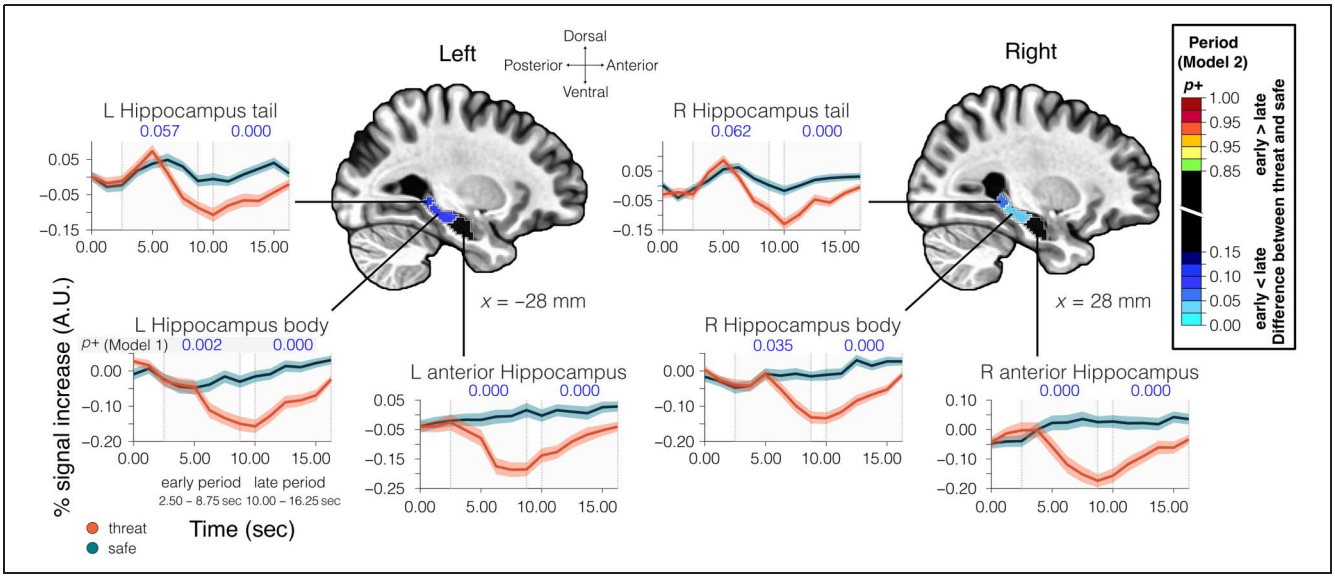

Figure 11. Estimated responses in the hippocampus (ROI level). Error bands show 95% interval for standard error across participants to illustrate variability only. Shaded regions indicate early and late periods. The strength of the effect of trial type is indicated separately for the early and late periods (see $p+$ values; colored font highlights the strongest effects). The effect of trial period is indicated via color coding of the ROIs (see color scale).

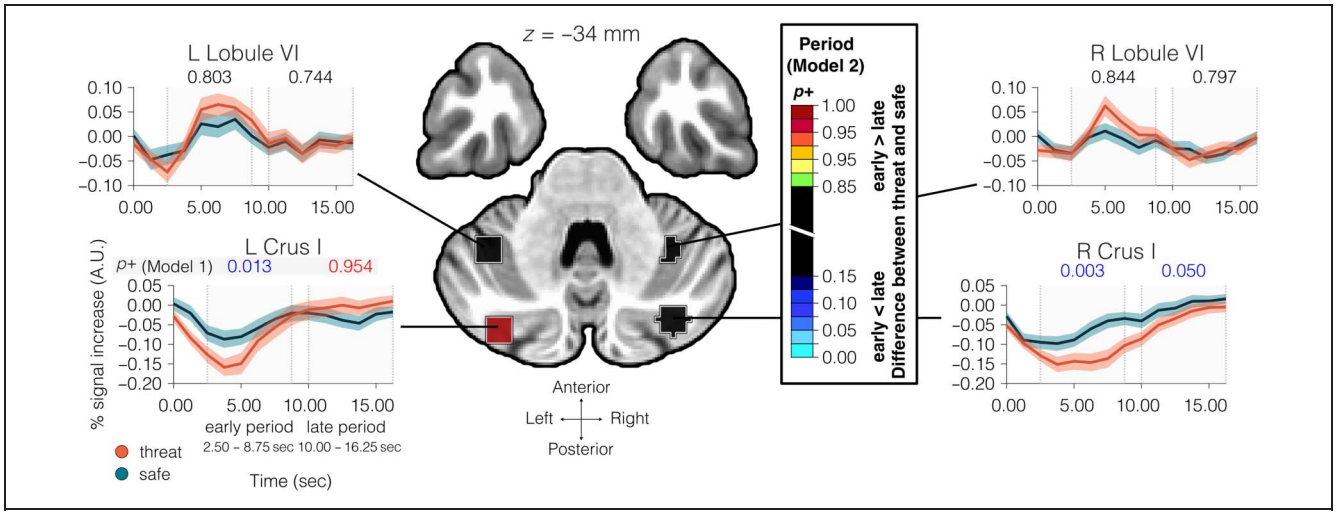

Figure 12. Estimated responses in the cerebellum (ROI level). Error bands show 95% interval for standard error across participants to illustrate variability only. Shaded regions indicate early and late periods. The strength of the effect of trial type is indicated separately for the early and late periods (see $p+$ values; colored font highlights the strongest effects). The effect of trial period is indicated via color coding of the ROIs (see color scale).

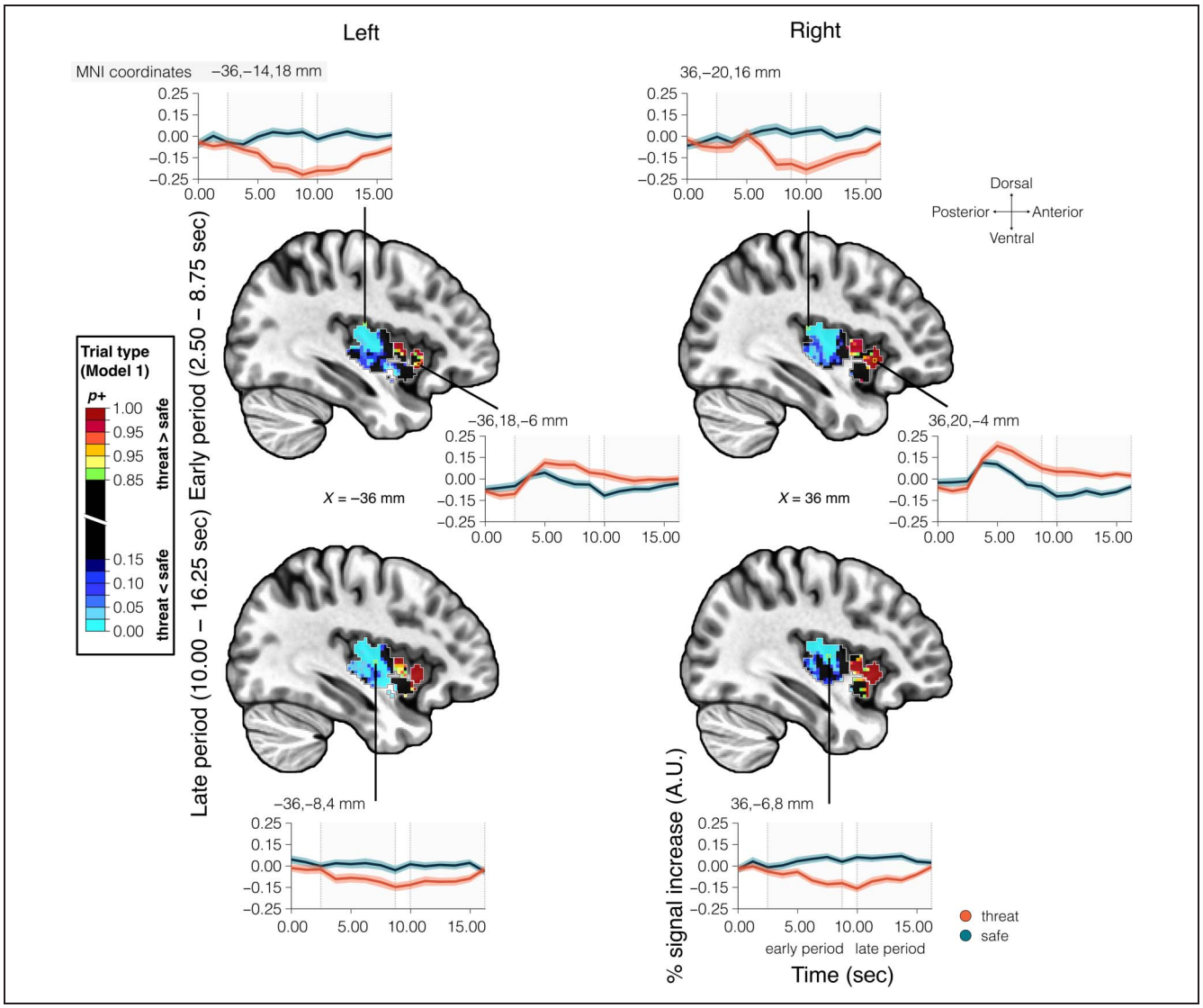

Figure 13. Estimated responses in the insula (voxel level). Error bands show 95% interval for standard error across participants to illustrate variability only. Shaded regions indicate early and late periods. The strength of the effect of trial type is indicated via color coding at the voxel level (see color scale).

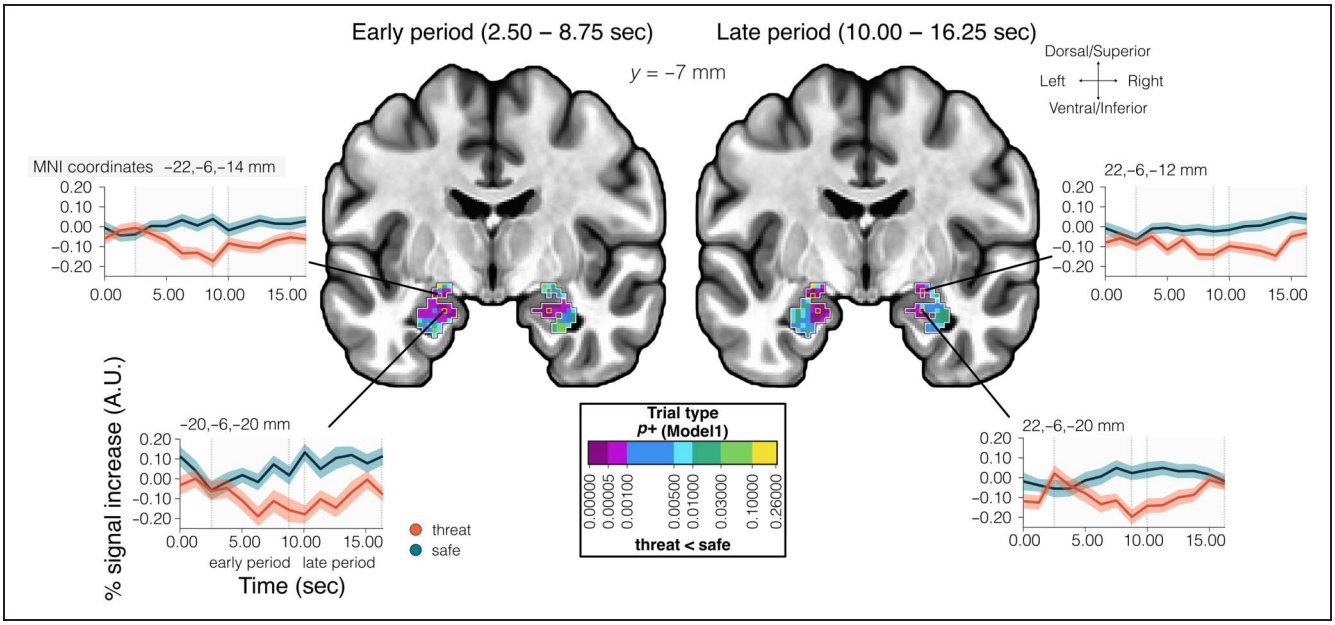

Figure 14. Estimated responses in the amygdala (voxel level). Error bands show 95% interval for standard error across participants to illustrate variability only. Shaded regions indicate early and late periods. The strength of the effect of trial type is indicated via color coding at the voxel level (see color scale).

and late periods uncovered regions for which period was an important factor (Figures 4 and 5). Figure 6 shows estimated responses for some of the regions with the strongest evidence of a condition effect, including both stronger responses during threat and during safe trials. Next, we examine the pattern of responses for some key brain regions.

Figure 7 shows responses during safe and threat trials in the insula. In the anterior dorsal insula, a stronger response to threat compared with safe was observed in the early period that extended into the late period. In the anterior ventral insula, we did not observe evidence for differential responses. A qualitatively different pattern of responses was observed in the middle/posterior insula, where signals increased in the early period for both threat and safe trials but then decreased for threat in the late period. Note that the color bar on the right indicates the strength of the period effect (early/late), which was relatively weak for all subparts of the insula. Figure 8 shows responses of two amygdala ROIs. Both centromedial and basolateral/basomedial amygdala did not generate prominent response increases to threat; in fact, differential responses were observed in the opposite direction (threat < safe). Figures 9 and 10 show responses in thalamus and striatum ROIs, where some of the strongest evidence of a period effect was observed. Figure 11 illustrates responses in the hippocampus, where responses resembled those in the amygdala to some extent. Figure 12 shows responses in the cerebellum.

Voxelwise Analysis

At present, whole-brain voxelwise BML analysis is not computationally feasible. Accordingly, to characterize the spatial distribution of the effects, we performed voxelwise analysis in two regions important for threat-related processing, namely, the insula and the amygdala. The results were in line with those in the ROI-level analyses. In the insula, increased responses with threat were observed almost entirely in the dorsal anterior sector (Figure 13). In contrast, in the posterior insula, responses were stronger during safe blocks. For the amygdala (Figure 14), the results followed the one found with the ROI-level analysis, but a spatial pattern of effect strength was also evident, with stronger evidence of differential responses particularly in more dorsal parts of the amygdala.

DISCUSSION

In this study, we examined how a period of sustained threat is processed in the human brain. We used a relatively large sample size (n = 109) and employed a Bayesian multilevel analysis approach to investigate responses across ROIs. Our results revealed that the effect of anxious apprehension is distributed across the brain and that the temporal evolution of the responses is quite varied, including more transient and more sustained profiles, as well as signal increases and decreases with threat. Overall, the impact of threat was widespread and not restricted to a small set of regions, such as the amygdala and the BST.

Big Picture

- Extended, uncertain threat engages the brain in a distributed fashion that prepares the organism to deal with the challenge. We believe that the focus on a few "typical" threat/aversive processing brain regions provides an impoverished and possibly misleading picture.

- Periods of anxious apprehension likely engage multiple mental processes, including those traditionally described as attentional, motivational, emotional, and action related. Whereas there is value in attempting to isolate some of these processes (e.g., "purely" emotional), in more natural settings, they are jointly engaged and likely intertwined. We believe that always trying to disentangle them is counterproductive.
- Transitioning between threat and safe states, and vice versa, leads to a massive switch in brain responding likely involving most of the brain.
- Responses during threat and safe states are complex and multifaceted, involving both signal increase and decrease, as well as different patterns of transient and sustained signals.

Key Findings

- Whereas some brain regions were engaged by threat, others were disengaged. Understanding both classes is necessary for a fuller appreciation of how the brain handles these states.
- Consistent with some, but not all, of the prior literature in humans, the amygdala was not engaged robustly during extended, uncertain threat.
- The bed nucleus of the stria terminalis was recruited transiently, not in a sustained fashion during threat.
- Regions that are part of the default network showed decreased responses during threat. It is possible that they disengage as the individual switches from self-related processing during safe conditions to preoccupation with the potential shock during threat.
- Some regions that showed decreased responses with threat (in comparison to safe blocks) may encode relative safety. Given evidence in rodents, this is possibly the case in the posterior insula.
- Responses often did not conform to canonical response shapes. Instead they showed nuanced/complex response profiles.

Caveats

- Because participants did not perform a task during threat/safe trials, interpretation of the underlying processes is challenging.
- For example, interpretation of the responses in the posterior insula in terms of safety is speculative, despite related findings in rodents.

Threat > Safe

During threat trials, increased responses were observed in multiple brain regions. Evidence of "transient" responses was very strong in, among others, multiple sectors of the inferior frontal gyrus (IFG), anterior MCC, pre-SMA, dorsolateral PFC, dorsal anterior insula, thalamus, and caudate. Evidence of "sustained" responses was strongest in different sectors of the inferior frontal, dorsal anterior insula, posterior MCC, dorsolateral PFC, and putamen. Several of these brain regions overlap with sites observed in pathological anxiety, consistent with the idea that induced states of apprehension may provide a useful model of some anxiety disorders (see Chavanne & Robinson, 2021).

An extensive literature has described the engagement of the anterior MCC in aversive processing (for a review, see Vogt, 2005). Current evidence supports the idea that the anterior MCC is involved in emotion-, cognition-, and pain-related processing (Shackman, Slagter, Fox, Winter, & Davidson, 2011; see also Misra & Coombes, 2015). In addition, meta-analyses suggest that the anterior MCC plays a central, integrative role in emotion regulation (Kohn et al., 2014) and is part of a core system for implementing self-control across emotion and action domains (Langner, Leiberg, Hoffstaedter, & Eickhoff, 2018). This study adds to this literature by showing that this region is transiently engaged when a threat context is initially experienced and closely replicates a previous finding by our lab (McMenamin et al., 2014) and also others (Hasler et al., 2007; Schlund et al., 2013); for evidence of a more sustained response profile, see Alvarez et al. (2011) and Hur et al. (2020).

Several conceptual frameworks implicate the anterior insula in the processing of sustained threat and have suggested that altered processing of this area underlies anxiety disorders (Robinson, Pike, Cornwell, & Grillon, 2019; Picó-Pérez, Radua, Steward, Menchón, & Soriano-Mas, 2017; Paulus & Stein, 2006). The dorsal anterior insula, particularly on the right, exhibited sustained responses that were greater for threat, consistent with many other studies (Somerville et al., 2013; Alvarez et al., 2011). Notably, we observed enhanced responses during threat only in the dorsal, not ventral, anterior insula. These results are in contrast with proposals that suggest that the ventral anterior insula is more engaged by emotion-related processing, whereas the dorsal sector is more recruited by cognitive-related processing (Uddin, Nomi, Hébert-Seropian, Ghaziri, & Boucher, 2017; Kurth, Zilles, Fox, Laird, & Eickhoff, 2010).

Although the present experiment was conceptualized as a study of temporally uncertain threat, it shares several features with "instructed fear" paradigms in which participants are told that a given stimulus will be followed by a stressor. These paradigms are believed to uncover brain regions that are important for the conscious appraisal of threat, including the MCC, anterior insula, and striatum (Mechias, Etkin, & Kalisch, 2010). It is noteworthy that, in our study, both the anterior insula and the posterior midcingulate exhibited increased responses during threat trials that persisted into the late period. It is also noteworthy that such sustained increased responses were observed in the anterior/superior ventral thalamus, anterior caudate, and

anterior putamen—regions consistently engaged during instructed fear studies (Mechias et al., 2010).

In the past two decades, there has been substantial interest in the potential roles of the BST in sustained "anxious/apprehensive" processing (Davis, Walker, Miles, & Grillon, 2010; Walker et al., 2003; Davis & Shi, 1999), and research in humans has accelerated considerably (Hur et al., 2020; McMenamin et al., 2014; Somerville et al., 2013; Alvarez et al., 2011). Whereas we had anticipated responses in the BST to exhibit a sustained response profile during threat trials, they were rather transient. Although unexpected, the present results indicate that, in some cases, BST responses are not sustained. In this study, instead, a more sustained pattern was observed for some cortical regions, including the dorsal anterior insula.

At present, there are increasing efforts to understand how distributed/large-scale circuits are involved in threat processing. For example, in a review of fear and anxiety, Tovote et al. (2015) described the participation of the amygdala, hippocampus, hypothalamus, PAG, thalamus, BST, medial PFC, and ventral striatum (including subregions of these structures), among others. Furthermore, it has been proposed that circuits involving multiple amygdala nuclei, PAG, medial PFC, and ventral striatum/nucleus accumbens participate in resolving between escape and freezing behavioral alternatives (LeDoux, Moscarello, Sears, & Campese, 2017; Moscarello & Hartley, 2017; Ilango, Shumake, Wetzel, & Ohl, 2014; Moscarello & LeDoux, 2013). In this context, we observed robust responses to threat in the striatum, in both the anterior caudate and the anterior putamen (both regions exhibited sustained responses); see also Pohlack, Nees, Ruttorf, Schad, and Flor (2012) for the involvement of the ventral striatum in contextual conditioning. Note that because the early/late periods did not require a response and because both conditions required the same type of motor response (button press) during the rating phase of trials, it is unlikely that differential responses were substantially driven by motor-related processing.

Threat < Safe

Whereas multiple brain regions respond vigorously when stressors are encountered, it is also noteworthy that some brain regions respond more strongly to safe relative to threat, as observed here and in other studies (Limbachia et al., 2021; Mobbs et al., 2010). As fMRI signals do not have an inherent baseline (Gusnard & Raichle, 2001), investigators must rely on contrasts, which allow them to test for differential responses such as threat < safe. In this study, we estimated responses without making hemodynamic assumptions, which provided qualitative information of the temporal evolution of the responses. In this manner, it was possible to clarify whether differential responses for threat < safe were due to a signal increase during safe trials or, instead, because of a signal decrease during threat trials.

In our study, because no task was required during the key part of the trial, it is possible that weaker responses during threat were related to routine processing in default network regions. The idea is that a region (e.g., PCC) is engaged during periods without an overt task, such as during a safe trial. However, during a threat trial, these regions are not recruited as strongly because the individual is now preoccupied with the potential unpleasant stimulation (consequently, the signal decreases during threat). Whereas several brain regions with robust threat < safe responses overlapped with the default network, some did not (overlap was assessed by comparing ROIs to default network masks of the parcellation by Schaefer et al., 2018). For example, the medial OFC ROI was entirely more ventral relative to parts of the medial OFC that are observed in the default network. The ROI that we called IFG 2 (see Figure 2) had very minimal overlap (a few voxels) with the default network. Among subcortical regions, threat < safe responses were observed in the ventral thalamus, posterior caudate, and parts of the cerebellum not typically linked to the default network.

In a previous study of threat controllability in humans, we observed responses in the posterior insula that were stronger during controllable relative to uncontrollable shocks (Limbachia et al., 2021). These findings were notable because in a threat controllability study in rodents, the posterior insula was suggested to encode a safety signal (Christianson et al., 2011). In this study, both the ROI level and the voxelwise Bayesian analyses uncovered responses greater for safe relative to threat, consistent with the notion that the posterior insula is involved in signaling a state of relative safety.

The status of amygdala responses to "sustained" threat in humans is unclear. Whereas some investigators have reported increased responses (Schlund et al., 2013), several others have actually observed decreases (McMenamin et al., 2014; Choi, Padmala, & Pessoa, 2012; Wager et al., 2009; Pruessner et al., 2008). Intriguingly, even in conditioning paradigms, the involvement of the amygdala is observed inconsistently (Fullana et al., 2018), possibly because of response habituation in this structure (Marschner, Kalisch, Vervliet, Vansteenwegen, & Büchel, 2008). Here, we observed greater responses for safe relative to threat in all amygdala ROIs. Furthermore, the response evolution indicated that signals during threat decreased relative to safe during the early period and remained lower during part of the late period. The voxelwise analysis confirmed these results, demonstrating that they did not result from the ROI-averaging process, while revealing that the most robust differences were located in relatively dorsal parts. Thus, in line with several other imaging studies, under the conditions of extended, uncertain threat of our experiment, the amygdala did not exhibit increased responses (but see Hur et al., 2020).

Study Limitations

We sought to investigate the brain correlates of anxious apprehension in the absence of a task to characterize

implicit brain responses. Periods of anxious apprehension likely engage multiple mental processes, including those traditionally described as attentional, motivational, emotional, and action related. Accordingly, in this study, we cannot attribute differential responses more directly to specific processes (but see Big Picture section). In particular, it is challenging to interpret the responses when responses are larger during safe versus threat trials, but when this difference is due to a relative decrease in signal during threat trials. Are some of these differential responses related to safety-related processing, as suggested for the posterior insula, for example, or other processes explain such pattern?

Although we collected anxiety ratings at the end of every trial, we were unable to utilize this information because ratings were highly correlated with trial condition, such that they did not carry independent information (participants mostly rated safe trials a level of 1 and threat trials a level greater than 1; see Figure 1C). Finally, in our experiment, the two trial types (threat, safe) were indicated by circles of different color (yellow and blue) but the colors were not counterbalanced across participants. Although this introduces a confound, our central goal was to study brain regions outside visual cortex that are not typically sensitive to stimulus color. Accordingly, we do not believe the lack of counterbalancing contributed substantially to differential responses.

Conclusion

This study investigated sustained threat-related processing across brain regions previously discussed in the literature. We employed BML to estimate effects when comparing periods of threat relative to periods of relative safety. At the broadest level, our study showed that periods of uncertain threat engage a broad, distributed set of brain regions, which display a diverse set of response profiles, including transient and sustained increased or decreased responses. Periods of anxious apprehension are likely to engage a number of mental processes, including those traditionally described as attentional, motivational, emotional, and action related, among others. Whereas there is value in attempting to isolate some of these processes (e.g., the more "purely" emotional), in more natural settings, they are jointly present and likely intertwined (Pessoa, Medina, & Desfilis, 2022). In this context, we observed a rich repertoire of response patterns during both threat and safe states, uncovering the multifaceted ways in which the brain is engaged during these states.

Acknowledgments

We acknowledge Chirag Limbachia for work on data analysis during early stages of this project and thank Gang Chen for discussions concerning statistical analysis.

Reprint requests should be sent to Luiz Pessoa, Department of Psychology, University of Maryland, College Park, MD, or via e-mail: pessoa@umd.edu.

Author Contributions

Dinavahi V. P. S. Murty: Formal analysis. Songtao Song: Formal analysis. Kelly Morrow: Formal analysis. Jongwan Kim: Formal analysis. Kesong Hu: Formal analysis. Luiz Pessoa: Conceptualization; Funding acquisition; Project administration; Supervision; Writing—Original draft.

Funding Information

Luiz Pessoa: National Institute of Mental Health (https://dx.doi.org/10.13039/100000025), grant number: R01 MH071589.

Diversity in Citation Practices

Retrospective analysis of the citations in every article published in this journal from 2010 to 2021 reveals a persistent pattern of gender imbalance: Although the proportions of authorship teams (categorized by estimated gender identification of first author/last author) publishing in the *Journal of Cognitive Neuroscience* (*JoCN*) during this period were M(an)/M = .407, W(oman)/M = .32, M/W = .115, and W/W = .159, the comparable proportions for the articles that these authorship teams cited were M/M = .549, W/M = .257, M/W = .109, and W/W = .085 (Postle and Fulvio, *JoCN*, 34:1, pp. 1–3). Consequently, *JoCN* encourages all authors to consider gender balance explicitly when selecting which articles to cite and gives them the opportunity to report their article's gender citation balance.

REFERENCES

Alvarez, R. P., Chen, G., Bodurka, J., Kaplan, R., & Grillon, C. (2011). Phasic and sustained fear in humans elicits distinct patterns of brain activity. *Neuroimage*, *55*, 389–400. https://doi.org/10.1016/j.neuroimage.2010.11.057, PubMed: 21111828

Amunts, K., Mohlberg, H., Bludau, S., & Zilles, K. (2020). Julich-Brain: A 3D probabilistic atlas of the human brain's cytoarchitecture. *Science*, *369*, 988–992. https://doi.org/10.1126/science.abb4588, PubMed: 32732281

Avants, B., Tustison, N., & Song, G. (2009). Advanced normalization tools: V1.0. *Insight Journal*, *618*

Boeke, E. A., Moscarello, J. M., LeDoux, J. E., Phelps, E. A., & Hartley, C. A. (2017). Active avoidance: Neural mechanisms and attenuation of Pavlovian conditioned responding. *Journal of Neuroscience*, *37*, 4808–4818. https://doi.org/10.1523/JNEUROSCI.3261-16.2017, PubMed: 28408411

Bürkner, P.-C. (2017). brms: An R package for Bayesian multilevel models using Stan. *Journal of Statistical Software*, *80*. https://doi.org/10.18637/jss.v080.i01

Canteras, N. S., Resstel, L. B., Bertoglio, L. J., de Pádua Carobrez, A., & Guimaraes, F. S. (2009). Neuroanatomy of anxiety. *Behavioral Neurobiology of Anxiety and Its Treatment*, 77–96. https://doi.org/10.1007/7854_2009_7, PubMed: 21309107

Chavanne, A. V., & Robinson, O. J. (2021). The overlapping neurobiology of induced and pathological anxiety: A meta-analysis of functional neural activation. *American Journal of Psychiatry*, *178*, 156–164. https://doi.org/10.1176/appi.ajp.2020.19111153, PubMed: 33054384

Chen, G., Saad, Z. S., Adleman, N. E., Leibenluft, E., & Cox, R. W. (2015). Detecting the subtle shape differences in hemodynamic responses at the group level. *Frontiers in Neuroscience*, *9*, 375. https://doi.org/10.3389/fnins.2015.00375, PubMed: 26578853

Chen, G., Taylor, P. A., Stoddard, J., Cox, R. W., Bandettini, P. A., & Pessoa, L. (2021). Dichotomous thinking and informational waste in neuroimaging. *BioRxiv*. https://doi.org/10.1101/2021.05.09.443246

Chen, G., Xiao, Y., Taylor, P. A., Rajendra, J. K., Riggins, T., Geng, F., et al. (2019). Handling multiplicity in neuroimaging through Bayesian lenses with multilevel modeling. *Neuroinformatics*, *17*, 515–545. https://doi.org/10.1007/s12021-018-9409-6, PubMed: 30649677

Choi, J. M., Padmala, S., & Pessoa, L. (2012). Impact of state anxiety on the interaction between threat monitoring and cognition. *Neuroimage*, *59*, 1912–1923. https://doi.org/10.1016/j.neuroimage.2011.08.102, PubMed: 21939773

Christianson, J. P., Jennings, J. H., Ragole, T., Flyer, J. G. N., Benison, A. M., Barth, D. S., et al. (2011). Safety signals mitigate the consequences of uncontrollable stress via a circuit involving the sensory insular cortex and bed nucleus of the stria terminalis. *Biological Psychiatry*, *70*, 458–464. https://doi.org/10.1016/j.biopsych.2011.04.004, PubMed: 21684526

Cox, R. W. (1996). AFNI: software for analysis and visualization of functional magnetic resonance neuroimages. *Computers and Biomedical Research*, *29*, 162–173. https://doi.org/10.1006/cbmr.1996.0014, PubMed: 8812068

Cremers, H. R., Wager, T. D., & Yarkoni, T. (2017). The relation between statistical power and inference in fMRI. *PLoS One*, *12*, e0184923. https://doi.org/10.1371/journal.pone.0184923, PubMed: 29155843

Davis, M., & Shi, C. (1999). The extended amygdala: Are the central nucleus of the amygdala and the bed nucleus of the stria terminalis differentially involved in fear versus anxiety? *Annals of the New York Academy of Sciences*, *877*, 281–291. https://doi.org/10.1111/j.1749-6632.1999.tb09273.x, PubMed: 10415655

Davis, M., Walker, D. L., Miles, L., & Grillon, C. (2010). Phasic vs sustained fear in rats and humans: Role of the extended amygdala in fear vs anxiety. *Neuropsychopharmacology*, *35*, 105–135. https://doi.org/10.1038/npp.2009.109, PubMed: 19693004

Desikan, R. S., Ségonne, F., Fischl, B., Quinn, B. T., Dickerson, B. C., Blacker, D., et al. (2006). An automated labeling system for subdividing the human cerebral cortex on MRI scans into gyral based regions of interest. *Neuroimage*, *31*, 968–980. https://doi.org/10.1016/j.neuroimage.2006.01.021, PubMed: 16530430

Destrieux, C., Fischl, B., Dale, A., & Halgren, E. (2010). Automatic parcellation of human cortical gyri and sulci using standard anatomical nomenclature. *Neuroimage*, *53*, 1–15. https://doi.org/10.1016/j.neuroimage.2010.06.010, PubMed: 20547229

Ezra, M., Faull, O. K., Jbabdi, S., & Pattinson, K. T. (2015). Connectivity-based segmentation of the periaqueductal gray matter in human with brainstem optimized diffusion MRI: Segmentation of the PAG with Diffusion MRI. *Human Brain Mapping*, *36*, 3459–3471. https://doi.org/10.1002/hbm.22855, PubMed: 26138504

Faillenot, I., Heckemann, R. A., Frot, M., & Hammers, A. (2017). Macroanatomy and 3D probabilistic atlas of the human insula. *Neuroimage*, *150*, 88–98. https://doi.org/10.1016/j.neuroimage.2017.01.073, PubMed: 28179166

Fan, L., Li, H., Zhuo, J., Zhang, Y., Wang, J., Chen, L., et al. (2016). The human brainnetome Atlas: A new brain atlas based on connectional architecture. *Cerebral Cortex*, *26*, 3508–3526. https://doi.org/10.1093/cercor/bhw157, PubMed: 27230218

Friston, K. J., Ashburner, J., Kiebel, S. J., Nichols, T. E., & Penny, W. D. (Eds.). (2007). *Statistical parametric mapping: The analysis of functional brain images*. Cambridge, MA: Academic Press. https://doi.org/10.1016/B978-012372560-8/50002-4

Fullana, M. A., Albajes-Eizagirre, A., Soriano-Mas, C., Vervliet, B., Cardoner, N., Benet, O., et al. (2018). Fear extinction in the human brain: A meta-analysis of fMRI studies in healthy participants. *Neuroscience & Biobehavioral Reviews*, *88*, 16–25. https://doi.org/10.1016/j.neubiorev.2018.03.002, PubMed: 29530516

Gelman, A. (2009). Bayes, Jeffreys, prior distributions and the philosophy of statistics. *Statistical Science*, *24*, 176–178. https://doi.org/10.1214/09-sts284d

Gelman, A., & Hill, J. (2006). Data analysis using regression and multilevel/hierarchical models. Cambridge: Cambridge University Press. https://doi.org/10.1017/cbo9780511790942

Grupe, D. W., & Nitschke, J. B. (2013). Uncertainty and anticipation in anxiety: An integrated neurobiological and psychological perspective. *Nature Reviews Neuroscience*, *14*, 488–501. https://doi.org/10.1038/nrn3524, PubMed: 23783199

Gusnard, D. A., & Raichle, M. E. (2001). Searching for a baseline: Functional imaging and the resting human brain. *Nature Reviews Neuroscience*, *2*, 685–694. https://doi.org/10.1038/35094500, PubMed: 11584306

Hasler, G., Fromm, S., Alvarez, R. P., Luckenbaugh, D. A., Drevets, W. C., & Grillon, C. (2007). Cerebral blood flow in immediate and sustained anxiety. *Journal of Neuroscience*, *23*, 6313–6319. https://doi.org/10.1523/jneurosci.5369-06.2007, PubMed: 17554005

Hermans, E. J., Henckens, M. J. A. G., Joëls, M., & Fernández, G. (2014). Dynamic adaptation of large-scale brain networks in response to acute stressors. *Trends in Neurosciences*, *37*, 304–314. https://doi.org/10.1016/j.tins.2014.03.006, PubMed: 24766931

Hermans, E. J., Van Marle, H. J. F., Ossewaarde, L., Henckens, M. J. A. G., Qin, S., Van Kesteren, M. T. R., et al. (2011). Stress-related noradrenergic activity prompts large-scale neural network reconfiguration. *Science*, *334*, 1151–1153. https://doi.org/10.1126/science.1209603, PubMed: 22116887

Hur, J., Smith, J. F., DeYoung, K. A., Anderson, A. S., Kuang, J., Kim, H. C., et al. (2020). Anxiety and the neurobiology of temporally uncertain threat anticipation. *Journal of Neuroscience*, *40*, 7949–7964. https://doi.org/10.1523/JNEUROSCI.0704-20.2020, PubMed: 32958570

Iglesias, J. E., Liu, C.-Y., Thompson, P. M., & Tu, Z. (2011). Robust brain extraction across datasets and comparison with publicly available methods. *IEEE Transactions on Medical Imaging*, *30*, 1617–1634. https://doi.org/10.1109/TMI.2011.2138152, PubMed: 21880566

Ilango, A., Shumake, J., Wetzel, W., & Ohl, F. W. (2014). Contribution of emotional and motivational neurocircuitry to cue-signaled active avoidance learning. *Frontiers in Behavioral Neuroscience*, *8*, 372. https://doi.org/10.3389/fnbeh.2014.00372, PubMed: 25386127

Kienast, T., Hariri, A. R., Schlagenhauf, F., Wrase, J., Sterzer, P., Buchholz, H. G., et al. (2008). Dopamine in amygdala gates limbic processing of aversive stimuli in humans. *Nature Neuroscience*, *11*, 1381–1382. https://doi.org/10.1038/nn.2222, PubMed: 18978778

Klumpers, F., Kroes, M. C. W., Baas, J. M. P., & Fernández, G. (2017). How human amygdala and bed nucleus of the stria terminalis may drive distinct defensive responses. *Journal of Neuroscience*, *37*, 9645–9656. https://doi.org/10.1523/jneurosci.3830-16.2017, PubMed: 28893930

Kohn, N., Eickhoff, S. B., Scheller, M., Laird, A. R., Fox, P. T., & Habel, U. (2014). Neural network of cognitive emotion

regulation—An ALE meta-analysis and MACM analysis. *Neuroimage*, *87*, 345–355. https://doi.org/10.1016/j.neuroimage.2013.11.001, PubMed: 24220041

Krienen, F. M., & Buckner, R. L. (2009). Segregated fronto-cerebellar circuits revealed by intrinsic functional connectivity. *Cerebral Cortex*, *19*, 2485–2497. https://doi.org/10.1093/cercor/bhp135, PubMed: 19592571

Kurth, F., Zilles, K., Fox, P. T., Laird, A. R., & Eickhoff, S. B. (2010). A link between the systems: Functional differentiation and integration within the human insula revealed by meta-analysis. *Brain Structure and Function*, *214*, 519–534. https://doi.org/10.1007/s00429-010-0255-z, PubMed: 20512376

Langner, R., Leiberg, S., Hoffstaedter, F., & Eickhoff, S. B. (2018). Towards a human self-regulation system: Common and distinct neural signatures of emotional and behavioural control. *Neuroscience & Biobehavioral Reviews*, *90*, 400–410. https://doi.org/10.1016/j.neubiorev.2018.04.022, PubMed: 29730485

LeDoux, J. E., Moscarello, J., Sears, R., & Campese, V. (2017). The birth, death and resurrection of avoidance: A reconceptualization of a troubled paradigm. *Molecular Psychiatry*, *22*, 24–36. https://doi.org/10.1038/mp.2016.166, PubMed: 27752080

Limbachia, C., Morrow, K., Khibovska, A., Meyer, C., Padmala, S., & Pessoa, L. (2021). Controllability over stressor decreases responses in key threat-related brain areas. *Communications Biology*, *4*, 1–11. https://doi.org/10.1101/2020.07.11.198762

Marschner, A., Kalisch, R., Vervliet, B., Vansteenwegen, D., & Büchel, C. (2008). Dissociable roles for the hippocampus and the amygdala in human cued versus context fear conditioning. *Journal of Neuroscience*, *28*, 9030–9036. https://doi.org/10.1523/JNEUROSCI.1651-08.2008, PubMed: 18768697

McElreath, R. (2018). *Statistical rethinking: A Bayesian course with examples in R and Stan*. Boca Raton, FL: Chapman & Hall/CRC. https://doi.org/10.1201/9781315372495

McMenamin, B. W., Langeslag, S. J. E., Sirbu, M., Padmala, S., & Pessoa, L. (2014). Network organization unfolds over time during periods of anxious anticipation. *Journal of Neuroscience*, *34*, 11261–11273. https://doi.org/10.1523/JNEUROSCI.1579-14.2014, PubMed: 25143607

Mechias, M.-L., Etkin, A., & Kalisch, R. (2010). A meta-analysis of instructed fear studies: Implications for conscious appraisal of threat. *Neuroimage*, *49*, 1760–1768. https://doi.org/10.1016/j.neuroimage.2009.09.040, PubMed: 19786103

Meyer, C., Padmala, S., & Pessoa, L. (2019). Dynamic threat processing. *Journal of Cognitive Neuroscience*, *31*, 522–542. https://doi.org/10.1101/183798, PubMed: 30513044

Misra, G., & Coombes, S. A. (2015). Neuroimaging evidence of motor control and pain processing in the human midcingulate cortex. *Cerebral Cortex*, *25*, 1906–1919. https://doi.org/10.1093/cercor/bhu001, PubMed: 24464941

Mobbs, D., Yu, R., Rowe, J. B., Eich, H., FeldmanHall, O., & Dalgleish, T. (2010). Neural activity associated with monitoring the oscillating threat value of a tarantula. *Proceedings of the National Academy of Sciences, U.S.A.*, *107*, 20582–20586. https://doi.org/10.1073/pnas.1009076107, PubMed: 21059963

Moscarello, J. M., & Hartley, C. A. (2017). Agency and the calibration of motivated behavior. *Trends in Cognitive Sciences*, *21*, 725–735. https://doi.org/10.1016/j.tics.2017.06.008, PubMed: 28693961

Moscarello, J. M., & LeDoux, J. E. (2013). Active avoidance learning requires prefrontal suppression of amygdala-mediated defensive reactions. *Journal of Neuroscience*, *33*, 3815–3823. https://doi.org/10.1523/jneurosci.2596-12.2013, PubMed: 23447593

Nacewicz, B. M., Alexander, A. L., Kalin, N. H., & Davidson, R. J. (2014). The neurochemical underpinnings of human amygdala volume including subregional contributions. *Biological Psychiatry*, *75*, 222S.

Paré, D., & Quirk, G. J. (2017). When scientific paradigms lead to tunnel vision: Lessons from the study of fear. *Npj Science of Learning*, *2*, 1–8. https://doi.org/10.1038/s41539-017-0007-4, PubMed: 30294453

Pauli, W. M., Nili, A. N., & Tyszka, J. M. (2018). A high-resolution probabilistic in vivo atlas of human subcortical brain nuclei. *Scientific Data*, *5*, 180063. https://doi.org/10.1038/sdata.2018.63, PubMed: 29664465

Pauli, W. M., O'Reilly, R. C., Yarkoni, T., & Wager, T. D. (2016). Regional specialization within the human striatum for diverse psychological functions. *Proceedings of the National Academy of Sciences, U.S.A.*, *113*, 1907–1912. https://doi.org/10.1073/pnas.1507610113, PubMed: 26831091

Paulus, M. P., & Stein, M. B. (2006). An insular view of anxiety. *Biological Psychiatry*, *60*, 383–387. https://doi.org/10.3171/2009.6.FOCUS09102, PubMed: 16780813

Pessoa, L., Medina, L., & Desfilis, E. (2022). Refocusing neuroscience: moving away from mental categories and towards complex behaviours. *Philosophical Transactions of the Royal Society B*, *377*, 20200534. https://doi.org/10.1098/rstb.2020.0534

Picó-Pérez, M., Radua, J., Steward, T., Menchón, J. M., & Soriano-Mas, C. (2017). Emotion regulation in mood and anxiety disorders: A meta-analysis of fMRI cognitive reappraisal studies. *Progress in Neuro-Psychopharmacology and Biological Psychiatry*, *79*, 96–104. https://doi.org/10.26226/morressier.5971be81d462b80290b52c31, PubMed: 28579400

Pohlack, S. T., Nees, F., Ruttorf, M., Schad, L. R., & Flor, H. (2012). Activation of the ventral striatum during aversive contextual conditioning in humans. *Biological Psychology*, *91*, 74–80. https://doi.org/10.1016/j.biopsycho.2012.04.004, PubMed: 22560888

Power, J. D., Mitra, A., Laumann, T. O., Snyder, A. Z., Schlaggar, B. L., & Petersen, S. E. (2014). Methods to detect, characterize, and remove motion artifact in resting state fMRI. *Neuroimage*, *84*, 320–341. https://doi.org/10.1016/j.neuroimage.2013.08.048, PubMed: 23994314

Pruessner, J. C., Dedovic, K., Khalili-Mahani, N., Engert, V., Pruessner, M., Buss, C., et al. (2008). Deactivation of the limbic system during acute psychosocial stress: Evidence from positron emission tomography and functional magnetic resonance imaging studies. *Biological Psychiatry*, *63*, 234–240. https://doi.org/10.1016/j.biopsych.2007.04.041, PubMed: 17686466

Pruim, R. H. R., Mennes, M., Buitelaar, J. K., & Beckmann, C. F. (2015). Evaluation of {ICA}-{AROMA} and alternative strategies for motion artifact removal in resting state {fMRI}. *Neuroimage*, *112*, 278–287. https://doi.org/10.1016/j.neuroimage.2015.02.063, PubMed: 25770990

Robinson, O. J., Pike, A. C., Cornwell, B., & Grillon, C. (2019). The translational neural circuitry of anxiety. *Journal of Neurology, Neurosurgery & Psychiatry*, *90*, 1353–1360. https://doi.org/10.1136/jnnp-2019-321400, PubMed: 31256001

Ruan, J., Bludau, S., Palomero-Gallagher, N., Caspers, S., Mohlberg, H., Eickhoff, S. B., et al. (2018). Cytoarchitecture, probability maps, and functions of the human supplementary and pre-supplementary motor areas. *Brain Structure and Function*, *223*, 4169–4186. https://doi.org/10.1007/s00429-018-1738-6, PubMed: 30187192

Schaefer, A., Kong, R., Gordon, E. M., Laumann, T. O., Zuo, X.-N., Holmes, A. J., et al. (2018). Local-global parcellation of the human cerebral cortex from intrinsic functional connectivity MRI. *Cerebral Cortex*, *28*, 3095–3114. https://doi.org/10.1093/cercor/bhx179, PubMed: 28981612

Schlund, M. W., Hudgins, C. D., Magee, S., & Dymond, S. (2013). Neuroimaging the temporal dynamics of human avoidance to sustained threat. *Behavioural Brain Research*, *257*, 148–155. https://doi.org/10.1016/j.bbr.2013.09.042, PubMed: 24095880

Scott, D. J., Heitzeg, M. M., Koeppe, R. A., Stohler, C. S., & Zubieta, J.-K. (2006). Variations in the human pain stress experience mediated by ventral and dorsal basal ganglia dopamine activity. *Journal of Neuroscience*, *26*, 10789–10795. https://doi.org/10.1523/JNEUROSCI.2577-06.2006, PubMed: 17050717

Shackman, A. J., & Fox, A. S. (2016). Contributions of the central extended amygdala to fear and anxietycontributions of the central extended amygdala to fear and anxiety. *Journal of Neuroscience*, *36*, 8050–8063. https://doi.org/10.1523/jneurosci.0982-16.2016, PubMed: 27488625

Shackman, A. J., Salomons, T. V., Slagter, H. A., Fox, A. S., Winter, J. J., & Davidson, R. J. (2011). The integration of negative affect, pain and cognitive control in the cingulate cortex. *Nature Reviews Neuroscience*, *12*, 154–167. https://doi.org/10.1038/nrn2994, PubMed: 21331082

Shattuck, D. W., & Leahy, R. M. (2002). BrainSuite: An automated cortical surface identification tool. *Medical Image Analysis*, *6*, 129–142. https://doi.org/10.1016/S1361-8415(02)00054-3, PubMed: 12045000

Smith, S. M., Jenkinson, M., Woolrich, M. W., Beckmann, C. F., Behrens, T. E. J., Johansen-Berg, H., et al. (2004). Advances in functional and structural MR image analysis and implementation as FSL. *Neuroimage*, *23 Suppl. 1*, S208–S219. https://doi.org/10.1016/j.neuroimage.2004.07.051, PubMed: 15501092

Somerville, L. H., Wagner, D. D., Wig, G. S., Moran, J. M., Whalen, P. J., & Kelley, W. M. (2013). Interactions between transient and sustained neural signals support the generation and regulation of anxious emotion. *Cerebral Cortex*, *23*, 49–60. https://doi.org/10.1093/cercor/bhr373, PubMed: 22250290

Spielberger, C. D., Gorsuch, R. L., Lushene, R. E., Vagg, P. R., & Jacobs, G. A. (1970). *Test manual for the State Trait Anxiety Inventory*. Mountain View, CA: Consulting Psychologists Press.

Sreenivasan, K. K., & D'Esposito, M. (2019). The what, where and how of delay activity. *Nature Reviews Neuroscience*, *20*, 466–481. https://doi.org/10.1038/s41583-019-0176-7, PubMed: 31086326

Theiss, J. D., Ridgewell, C., McHugo, M., Heckers, S., & Blackford, J. U. (2017). Manual segmentation of the human bed nucleus of the stria terminalis using 3 T MRI. *Neuroimage*, *146*, 288–292. https://doi.org/10.1016/j.neuroimage.2016.11.047, PubMed: 27876653

Thomason, M. E., Hamilton, J. P., & Gotlib, I. H. (2011). Stress-induced activation of the HPA axis predicts connectivity between subgenual cingulate and salience network during rest in adolescents. *Journal of Child Psychology and Psychiatry*, *52*, 1026–1034. https://doi.org/10.1111/j.1469-7610.2011.02422.x, PubMed: 21644985

Tian, Y., Margulies, D. S., Breakspear, M., & Zalesky, A. (2020). Topographic organization of the human subcortex unveiled with functional connectivity gradients. *Nature Neuroscience*, *23*, 1421–1432. https://doi.org/10.1038/s41593-020-00711-6, PubMed: 32989295

Toro, R., Fox, P. T., & Paus, T. (2008). Functional coactivation map of the human brain. *Cerebral Cortex*, *18*, 2553–2559. https://doi.org/10.1093/cercor/bhn014, PubMed: 18296434

Tovote, P., Fadok, J. P., & Lüthi, A. (2015). Neuronal circuits for fear and anxiety. *Nature Reviews Neuroscience*, *16*, 317–331. https://doi.org/10.1038/nrn3945, PubMed: 25991441

Uddin, L. Q., Nomi, J. S., Hébert-Seropian, B., Ghaziri, J., & Boucher, O. (2017). Structure and function of the human insula. *Journal of Clinical Neurophysiology*, *34*, 300. https://doi.org/10.1097/wnp.0000000000000377, PubMed: 28644199

Vogt, B. A. (2005). Pain and emotion interactions in subregions of the cingulate gyrus. *Nature Reviews Neuroscience*, *6*, 533–544. https://doi.org/10.1038/nrn1704, PubMed: 15995724

Wager, T. D., van Ast, V. A., Hughes, B. L., Davidson, M. L., Lindquist, M. A., & Ochsner, K. N. (2009). Brain mediators of cardiovascular responses to social threat, Part II: Prefrontal-subcortical pathways and relationship with anxiety. *Neuroimage*, *47*, 836–851. https://doi.org/10.1016/j.neuroimage.2009.05.044, PubMed: 19465135

Walker, D. L., Toufexis, D. J., & Davis, M. (2003). Role of the bed nucleus of the stria terminalis versus the amygdala in fear, stress, and anxiety. *European Journal of Pharmacology*, *463*, 199–216. https://doi.org/10.1016/s0014-2999(03)01282-2, PubMed: 12600711

Wojtasik, M., Bludau, S., Eickhoff, S. B., Mohlberg, H., Gerboga, F., Caspers, S., et al. (2020). Cytoarchitectonic characterization and functional decoding of four new areas in the human lateral orbitofrontal cortex. *Frontiers in Neuroanatomy*, *14*, 2. https://doi.org/10.3389/fnana.2020.00002, PubMed: 32116573

Yao, S., Qi, S., Kendrick, K. M., & Mobbs, D. (2018). Attentional set to safety recruits the ventral medial prefrontal cortex. *Scientific Reports*, *8*, 1–9. https://doi.org/10.1101/249326